August 1997 • NREL/SR-520-23404

High-Efficiency Thin-Film Cadmium Telluride Photovoltaic Cells

Annual Technical Report
20 January 1996 - 19 January 1997

A.D. Compaan, R.G. Bohn,
and G. Contreras-Puente
University of Toledo
Toledo, Ohio

National Renewable Energy Laboratory
1617 Cole Boulevard
Golden, Colorado 80401-3393
A national laboratory of
the U.S. Department of Energy
Managed by Midwest Research Institute
for the U.S. Department of Energy
under Contract No. DE-AC36-83CH10093

NREL/SR-520-23404 • UC Category: 1263

High-Efficiency Thin-Film Cadmium Telluride Photovoltaic Cells

Annual Technical Report 20 January 1996 - 19 January 1997

A.D. Compaan, R.G. Bohn,
and G. Contreras-Puente
University of Toledo
Toledo, Ohio

NREL technical monitor: B. von Roedern

National Renewable Energy Laboratory
1617 Cole Boulevard
Golden, Colorado 80401-3393
A national laboratory of
the U.S. Department of Energy
Managed by Midwest Research Institute
for the U.S. Department of Energy
under Contract No. DE-AC36-83CH10093

Prepared under Subcontract No. ZAX-4-14013-4

August 1997

NOTICE

Available to DOE and DOE contractors from:
Office of Scientific and Technical Information (OSTI)
P.O. Box 62
Oak Ridge, TN 37831
Prices available by calling (423) 576-8401

Available to the public from:
National Technical Information Service (NTIS)
U.S. Department of Commerce
5285 Port Royal Road
Springfield, VA 22161
(703) 487-4650

Printed on paper containing at least 50% wastepaper, including 20% postconsumer waste

SUMMARY

The University of Toledo photovoltaics group has been instrumental in developing rf sputtering for CdS/CdTe thin-film solar cells. During the third phase of the present contract our work focussed on efforts to determine factors which limit the efficiency in our "all-sputtered" thin-film CdTe solar cells on soda-lime glass. We find that our all-sputtered cells, which are deposited at substantially lower temperature than those by sublimation or vapor deposition, require less aggressive $CdCl_2$ treatments than do other deposition techniques and this is presumably related to CdS/CdTe interdiffusion. The CdS/CdTe interdiffusion process has been studied by several methods, including photoluminescence and capacitance-voltage measurements. Furthermore, we have deposited special thin bilayer films on quartz and borosilicate glass. Interdiffusion in these thin bilayers have been probed by Rutherford backscattering, with collaborators at Case Western Reserve University, and grazing incidence x-ray scattering (GIXS), with collaborators at the University at Buffalo and Brookhaven National Lab. Also, in order better to understand the properties of the ternary alloy material, we used laser physical vapor deposition to prepare a series of CdS_xTe_{1-x} films on borosilicate glass. The composition of the alloy films was determined by wavelength dispersive x-ray spectroscopy at NREL. These films are currently being investigated by us and other groups at NREL and IEC.

In addition to efforts focussed on factors which may be unique to rf sputtered cells, we participated in activites emphasizing common issues in CdTe thin film solar cells. Further participation in the CdTe Thin Film Teaming project with studies of thin CdS have yielded interesting results. For this effort we prepared cells on both 7059 borosilicate glass with conducting tin oxide layers deposited at the University of South Florida and on soda-lime glass with textured SnO_2:F from LOF. Including the work from the previous phase, we have now fabricated seven types of cells with CdS thicknesses of 300, 200, 100, 80, 60, 20, and 0 nm. For each CdS thickness, cells on the 7059 and soda lime superstrates were prepared side-by-side through all steps in the preparation to facilitate direct comparisons. The 7059/USF SnO_2 superstrates had much better performance for CdS thicknesses of 100 nm and below with the major differences occurring in the open circuit voltage. One set of cells prepared without CdS by sputtering CdTe directly on the 7059/USF SnO_2 superstrates showed an initial V_{OC} = 760 mV and initial efficiency of 8.7%.

Other characterization measurements in use at UT include temperature-dependent Hall effect and electrical conductivity, current-voltage (I-V), spectral quantum efficiency (SQE), and frequency-dependent capacitance-voltage (C-V) measurements.

Table of Contents

LIST OF FIGURES

LIST OF TABLES

1.0 Introduction

1.1 Background

This annual report covers the third year of a three-year NREL subcontract with the University of Toledo which is focussed on further developments in rf sputtering of CdS, CdTe, and related materials for improved thin-film solar cells on glass. This contract has now been extended into a fourth year. In earlier work supported by NREL, the University of Toledo established the viability of rf sputtering for thin-film CdS and CdTe by fabricating "all-sputtered" cells on soda-lime glass with AM 1.5 efficiencies of up to 11.6%.[1,2,3] Although rf sputtered cells have not yet reached the record efficiencies of close spaced sublimation, some of the work of the past year points toward the possibility of significant advances in all-sputtered cell efficiencies. Furthermore, even at the present state of the art, we have shown that the sputtering technique is advantageous in a number of ways, including the preparation of extremely thin layers and bilayers.

In addition to rf sputtering, the UT group continues to use laser physical vapor deposition (LPVD), often called pulsed laser deposition (PLD), as the method of choice for the deposition of $CdCl_2$ layers and also for the exploration of new materials such as the ternary alloys including CdS_xTe_{1-x} and dopants such as Cu in ZnTe.

1.2 Technical Approach

RF sputtering--The process of rf sputtering permits a considerable amount of flexibility in the deposition of CdS and CdTe. It is believed that the presence of significant densities of electrons, excited atoms and ions can be manipulated to improve the quality of the as-deposited films and/or lower the growth temperature due to the impact of energetic species on the film growth interface.[4] Much of our effort is designed to examine these effects with the ultimate goal of fabricating rf sputtered CdS/CdTe thin film solar cells with efficiencies exceeding 15% on soda-lime glass. In order to do this, it is important to obtain a thorough understanding of the fundamentals of the sputter-deposition process. We utilize a specially designed two-gun magnetron sputtering chamber with optical thickness monitors as described previously.[3,5] As discussed in our report for last year,[1] this chamber is now equipped with two, type II unbalanced magnetrons, with two-inch diameter targets.

The results of the CdTe teaming activity, including our own contributions have pointed toward the importance of the SnO_2/CdS interface and the use of a thin layer of intrinsic SnO_2. Thus, we have instrumented a second sputtering system during the past year which we have recently used for the sputter deposition i-SnO_2 on standard LOF Tec-8 glass substrates. The sputter gun was constructed at UT to provide us with maximum flexibility for adjusting the magnetic field of the magnetron.

$CdCl_2$ treatment and contacting--We have continued the use of laser physical vapor deposition (LPVD) for the $CdCl_2$ application followed by the usual anneal at ~385 °C in air. We have continued to do some work to explore the use of graphite-based contacts although to this point we have not

found better initial results than the diffused copper/evaporated gold contacts used in the past. Improved contacts remain an important goal for us. During the past six months we have been working to instrument broader capability for metallizations. We have installed a three-gun DC sputtering system in our laboratory. This versatile system was donated to UT by the Findlay, OH, plant of Harris Semiconductor[6] when they decomissioned it from their three-inch wafer fabrication line.

Materials characterization/device testing-- We continue to make extensive use of x-ray diffraction, Raman scattering, photoluminescence (PL), optical absorption, scanning tunnelling microscopy, and scanning electron microscopy with energy dispersive x-ray spectroscopy for studies of film morphology, structure, composition, and defects. We used four-point probe and van der Pauw measurements of conductivity as well as Hall effect measurements of carrier concentration and mobility. All fabricated devices are tested by current-voltage measurements, and some are tested for spectral quantum efficiency and by frequency-dependent capacitance-voltage measurements.

Exploratory and collaborative studies-- We continued collaboration during the past year with Mark Stan and Prof. Arthur Heuer at the Ion Beam Analysis Facility at Case Western Reserve University[7] for Rutherford backscattering (RBS) measurements of interdiffusion in CdS/CdTe bilayers on silica. In order to explore the CdS/CdTe interface and interface roughening with high sensitivity, we started a collaboration with the group of Prof. Yi Han Kao at the University at Buffalo (SUNY)[8] for grazing incidence x-ray scattering measurements at the Brookhaven National Laboratory. In addition to teaming activity as part of the "thin CdS" effort, we have done collaborative studies with IEC and with several scientists at NREL.

2.0 Advances in Film Deposition and Cell Fabrication

2.1 Increase in sputter deposition rates

Since the beginning of our sputtering work, we have been growing the CdS and CdTe films at very low rf power, ~25 W, which, for a two-inch target is an average power density of 1.2 W/cm^2. The growth rates were similar to those we had used for the pulsed laser deposition growth of these films. Our early work indicated that the growth rate during rf sputtering could not be increased more than about a factor of two above 5 Å/sec. (See Annual Report for 1995.)[1] However, as mentioned in our last annual report, we have recently eliminated a lossy element in our rf matching network, which had been dissipating much of the rf power before reaching the sputtering guns. We have now performed a study of growth rate vs. rf power as shown in Figure 2.1. From this study it is clear that the growth rate is linear in rf power above a threshold of about 15 watts. Thus we were able to reach a growth rate of 27 Å/sec with a power of 70 W into the 2 inch diameter sputtering gun (power density of 3.5 W/cm$^{2)}$. This growth rate was achieved even though our target-to-substrate distance is quite large (70 mm for a 50 mm target size). Thus a 2 μm film can be grown in just over 12 minutes. We did not try to push the growth rate higher because of concerns over heat flow into the target which was not bonded to a copper holder and no heat sinking compound was used to attach the target to the gun.

We have prepared one solar cell film (with about 20 small cells each) at several of the higher sputtering rates (with rf powers of 30, 40 and 50 W) and find no significant loss of performance at the higher rates. Thus, the cells grown at 50 W of power gave performances well above 10% by our tests. We are encouraged that these data indicate considerable promise for the commercial viability of the rf sputtering technique for thin-film CdTe cells. Even if our highest power density of 70 W/20 cm^2 = 3.5 W/cm^2 could not be exceeded for this type of sintered target, a scale-up to larger targets and substrates with similar target-to-substrate distance should improve the solid angle coverage by a factor of three or more with corresponding increase in deposition rate.

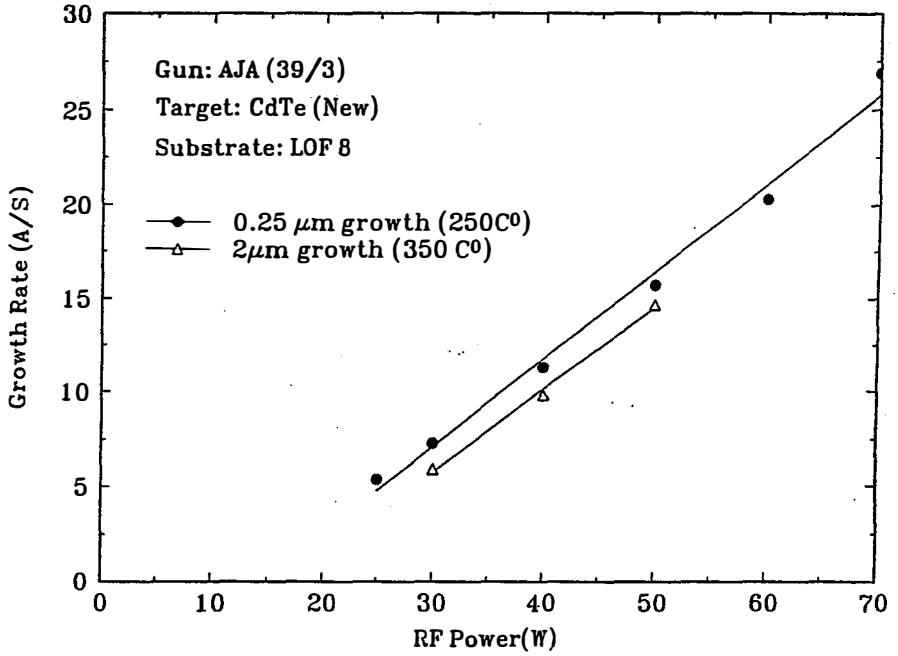

Fig. 2.1. Growth rate of CdTe vs. rf power at 250 °C and 350 °C.

Although early results appear to indicate that the film quality does not seriously degrade at sputtering rates five times higher than our usual, we anticipate that it optimum film quality at this rate and particularly at still higher rates may require either higher deposition temperatures or improved optimization and control of the ion-bombardment effects in the rf plasma.

2.2 Implementation of additional sputtering capabilities

As discussed below, much of the teaming activity points toward the advantages of using thinner CdS layers and indicates that thin CdS is best accompanied by an intrinsic transparent conducting oxide layer such as i-SnO_2. Our side-by-side growth of cells on substrates with and without an insulating SnO_2 layer, as part of the teaming activity in the last two rounds show clearly this effect. (See Section 3 below.) Therefore, we have recently rehabilitated our first, single gun, sputtering chamber for deposition of TCO layers. In order to implement this sytem, we built our own two-inch diameter sputter gun incorporating ceramic magnets from a Toledo-area supplier of NdFeB magnets, Dura Magnetics, Inc.[9] This system is now operational and we are currently in the process of optimizing the growth for the highest optical and electrical quality of TCO materials.

We have rf sputtered SnO_2 from a standard SnO_2 target both in pure argon and with small admixtures of oxygen. The resulting films on glass are transparent and highly resistive when depositions are made at ~200 °C. We are beginning to use sputtered i-SnO_2 layers on LOF Tec-8 glass for cell fabrication.

In addition, we acquired in the fall of 1996 a three-gun dc sputtering system donated from Harris Semiconductor of Findlay, OH. This system is presently being installed at U.T. and modified to allow the mounting of standard solar cells in such a way as to permit sequential deposition of up to three different materials.

3.0 CdTe Thin Film Partnership Teaming Activities

3.1 Thin CdS Team

During the previous contract year, the University of Toledo supplied eight cells as part of the teaming activity for studies of thin CdS. We reported some of those results in our annual report for that contract year. Comprehensive measurements on these cells, as well as on cells from other groups, were made at Colorado State University by Prof. Sites' group and reported at the 25th IEEE Photovoltaic Specialists Conference in May, 1996. We include part of that summary on UT cells below. This will provide a background for the discussion of additional cells which we supplied in the latest round of teaming activity. For the earlier round of activity, we supplied "all sputtered" cells with as-deposited CdS thicknesses of 200, 140, 70, and 40 nm (measured by our *in situ* optical transmission monitor). Cells were fabricated on both borosilicate glass superstrates (7059/USF) and on soda-lime glass superstrates (LOF/10Ω/□). For each thickness the two superstrates were mounted side-by-side in the deposition chamber on a stainless steel mounting jig. For further details see our previous annual report.[1] For the latest round, we again supplied cells on both types of superstrates, this time with as-deposited CdS thicknesses of 60, 20, and 0 nm. (In this case the soda-lime glass was LOF Tec-8, with slightly lower resistivity and slightly less haze than the LOF 10Ω/□.)

3.2 Thin sputtered CdS--BSG(7059)/USF vs. SLG/LOF superstrates

Since our usual superstrate size for sputter deposition is 2.75 x 3.0 inches and the standard size used with the teaming activity is approximately 1.25 x 1.25 inches, we seized the opportunity make side-by-side comparisons between the two types of superstrates: ~1 mm thick borosilicate glass with a multilayer SnO_2 deposited by Chris Ferekides' group at the University of South Florida[10] and 3 mm thick soda-lime glass from LOF with their Tec-8 or Tec-10 SnO_2 coating.

The results from the earlier round are summarized in Figs. 3.1 and 3.2. below, taken from Ref. 11. Interpretation of these data has been given in Ref. 11 which we excerpt below:

> [Fig. 3.1] compares the JV results for the UT cells. The top figure demonstrates the 7059 superstrates while the bottom figure shows the LOF superstrates. The JV data shown were taken at 25 °C. In both cases, the increase in J_{SC} with decreasing CdS

thickness is clear. However, V_{oc} and FF tend to decrease as the CdS is thinned. This effect is quite dramatic in the LOF case. In the UT cells it is clear that series resistance is increasing as the CdS is thinned, and a second-barrier "rollover" beyond V_{oc} becomes apparent for the thinner CdS cells.

QE is used to compare cell photocurrent performance for various CdS window-layer thicknesses. [Figure 3.2] demonstrates the results for the same UT cells. Again, the top figure depicts the 7059 superstrates while the bottom figure depicts the LOF superstrates. Also shown are the photon fractions lost to reflection (for the 700 Å-CdS cell on 7059 glass and for the 2000 Å-CdS cell on LOF glass) and to absorption

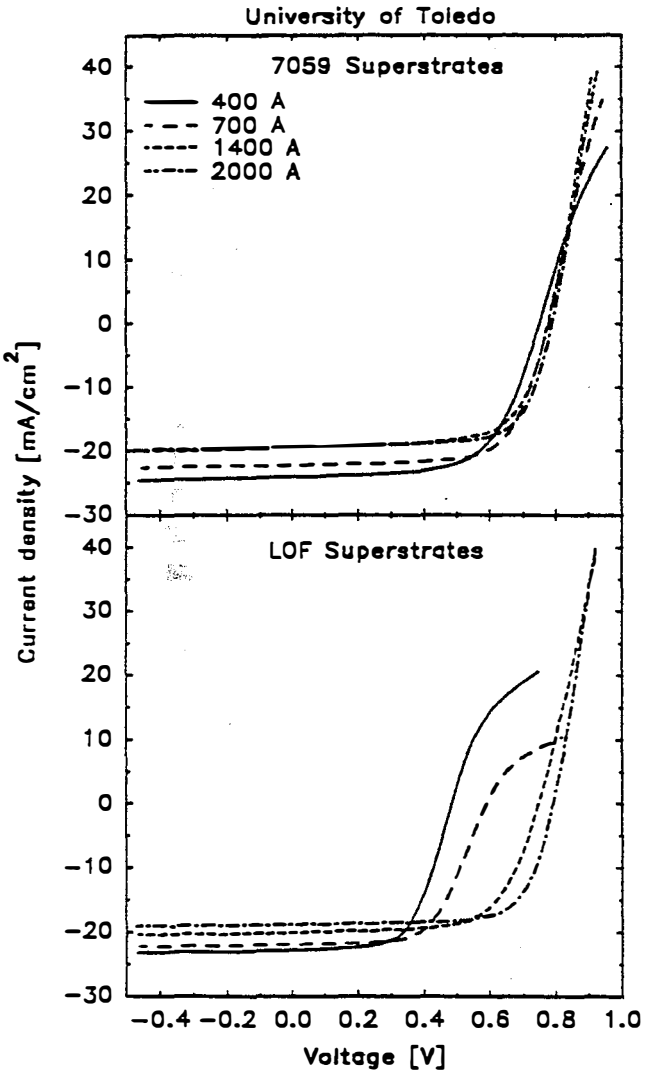

Fig. 3.1. Current-voltage data for rf sputtered cells. Light JV curves were measured at 25°C under an illumination of 100 mW/cm².

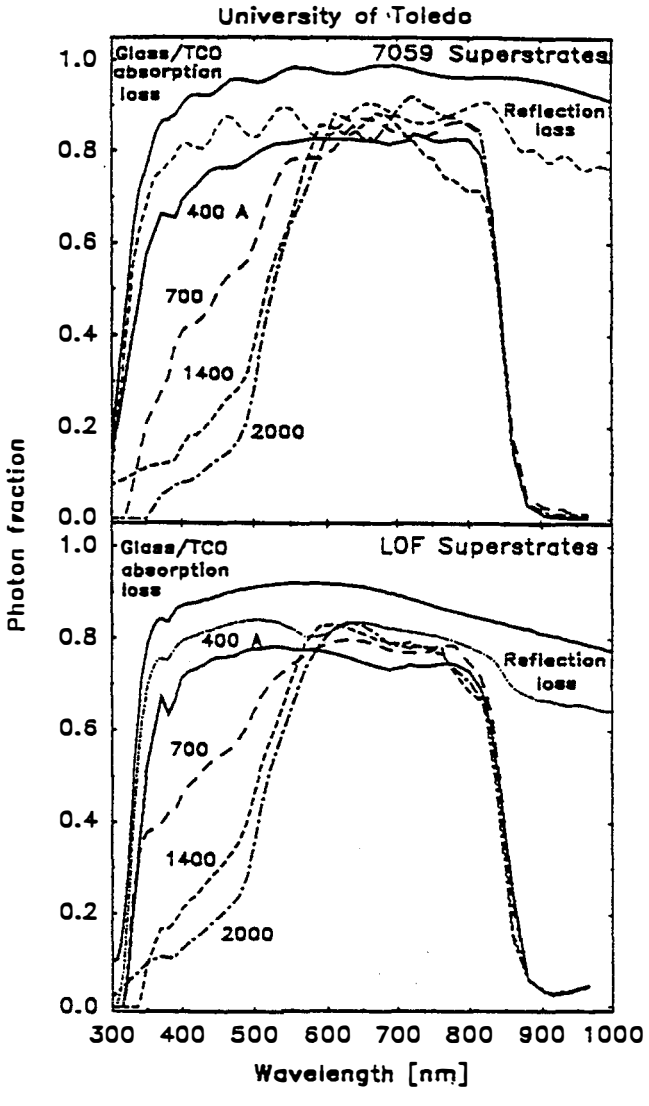

Fig. 3.2. Quantum efficiency data for rf sputtered cells. Data were measured at zero voltage bias under a white-light bias of 100 mW/cm².

in the glass/transparent-conducting-oxide (TCO) superstrate. The QE data shown were taken with a white light bias of 100 mW/cm^2, but curves taken without the bias light are essentially identical. The less pronounced interference in reflection and QE curves on the LOF glass is due to a coating designed to reduce spectral variation. The LOF/TCO superstrates have somewhat greater absorption and slightly lower reflection than the corresponding 7059 superstrates. The increased collection for photon energy above the CdS bandgap (wavelengths below 520 nm) as the CdS thickness decreases is obvious and is about the same for both types of glass. Also with both types of glass the thin (400 Å) CdS cell has a somewhat (~5%) lower QE between 550 nm and 750 nm. This may be due to increased recombination in these cells.

In the most recently completed round of thin CdS cell fabrication, we prepared six more cells as described above. These extend the structures to even thinner CdS and include two cells prepared with no CdS, *i.e.*, the CdTe is sputtered directly on the TCO layer for each type of superstrate.

The results are summarized in Tables 3.1 and 3.2 below. Table 3.1 shows measurements obtained at Colorado State University one to two months after cell fabrication. Table 3.2 shows a combination of measurements, some done in our lab immediately after fabrication and one set done at CSU.

Table 3.1. Comparison of cell performance on different substrates
(measured at Colorado State University, round 1)

[cell I.D.] **CdS thickness** [cell I.D.]	**superstrate type**	**V_{oc}(mV)**	**J_{sc}(mA/cm^2)**	**FF(%)**
[SSC303-14] **300 nm** [SSC303-18]	7059/USF	790	19.5	70
	LOF 8 Ω/□	800	19.0	70
[SSC304-7] **200 nm** [SSC304-12]	7059/USF	780	19.5	67
	LOF 8 Ω/□	755	20.0	65
[SSC305-14] **100 nm** [SSC305-11]	7059/USF	780	22.5	68
	LOF 8 Ω/□	600	22.0	60
[SSC306-21] **60 nm** [SSC306-17]	7059/USF	760	24	62
	LOF 8 Ω/□	490	23	60

Since we utilize an optical thickness monitor during growth, it is straightforward to control the CdS thickness. In addition, the sputtered CdTe grows easily on either type of SnO_2. The 1 mm 7059 superstrates are more transparent than the 3 mm LOF soda-lime. The USF coating is smoother and more transparent than the LOF and it is our understanding that the USF coating uses a final intrinsic layer of SnO_2. The availability of both types of cells with the wide range of CdS thicknesses presents an unusual opportunity to explore the role of CdS. It is known that

optical absorption in the CdS window layer can severely limit the cell current and finding ways to reduce it is a major objective of the teaming activity. In addition, it is important to understand the importance of interdiffusion in optimizing the cell performance. In this regard it is particularly interesting to be able to prepare cells with pure CdTe and no CdS layer at all. This we have done with the cells described in the two tables. Note that the tested cells had an area of 0.113 cm^2 and were selected from a structure with either 6 or 9 cells defined by the Cu/Au evaporation mask. It should be pointed out that our deposition temperature (380 °C) and postdeposition processing has been optimized with the LOF substrates and there is no reason to believe that the fabrication process on the 7059/USF superstrates is fully optimized. We have made fewer than ten deposition runs on the 7059 superstrates.

Table 3.2. Comparison of sputtered cell performance on different substrates
at Colorado State U round

[cell I.D.] CdS thickness [cell I.D.]	superstrate type	V_{oc}(mV)			J_{sc}(mA/cm²)			FF(%)		
		day 1	day 5	day 30‡	day 1	day 5	day 30‡	day 1	day 5	day 30‡
[SSC489-22] 80 nm [SSC489-14]	7059/USF	784	761	750	21.4	21.0	23.6	68.5	65.6	65
	LOF 8 Ω/□	623	595		19.9	20.3		59.5	58.5	
[SSC490-23] 20 nm [SSC490-13]	7059/USF	769	711	765	22.7	21.6	19.8	63.6	54.7	53
	LOF 8 Ω/□	511	435		19.9	19.7		64.4	61.2	
[SSC491-8] 0 nm [SSC491-24]	7059/USF	763	696*		20.1	19.2*		56.6	42.9*	
	LOF 8 Ω/□	473	414*		20.1	19.4*		57.4	57*	

* these cells were tested on day 2 ‡ measurement done > 30 days later at CSU

We find that the largest difference between the two types of superstrates is that the cells sputtered on 7059/USF had consistently higher V_{oc} than those on LOF. This voltage difference increased as the CdS thickness decreased. Note that with 300 nm of CdS the V_{oc} for the two types of superstrates are essentially the same, ~800 mV. However, for 60 nm of CdS or less the V_{oc} for LOF superstrates is 490 mV or less whereas for the USF superstrates, the V_{oc} is 696 mV or higher.

After our standard processing, which includes the LPVD $CdCl_2$ deposition and 385 °C anneal for 20 min in air, Cu/Au 4 mm diameter circular contacts were evaporated and diffused at 150 C for 30 min. (No etching was done.) As mentioned above, these diffused contacts are not stable and we monitored the performance of at least one cell on each film for a period of about two weeks before sending the cells to Colorado State University for testing.

Our measurements were done with an ELH lamp standardized to a Si reference cell and have an estimated absolute error of ±1% in efficiency (±10% relative error). Modeling the J-V curves indicates that the primary change with time is the apparent series resistance at AM 1.5. For the cell with 1000 Å CdS layer, the apparent series resistance increased from 3.6 Ω-cm^2 to 4.5 Ω-cm^2, whereas for the cell with 600 Å of CdS, the apparent series resistance increased from 4.0 Ω-cm^2 to 6.3 Ω-cm^2. We believe that the instability is wholly or, at least primarily, due to deterioration of the diffused Cu/Au contact.

Among the sets of CdS thicknesses supplied by five different groups for this teaming work, the UT cells covered the widest range of CdS thicknesses. The cell efficiencies at AM 1.5 fell in the middle of the range in this study. The UT group was the only group to supply cells on soda-lime glass as part of this study. It is interesting that for thick CdS (3000 and 2000 Å) our cells on soda-lime (LOF) glass outperformed our cells on the 7059 glass in spite of the fact that the 7059 glass is more transparent and the USF SnO_2 coating has less haze. We suggest that this may arise from the fact that our process has been optimized with the LOF glass.

Our conclusion is that the multilayer SnO_2 deposited by the University of South Florida is largely responsible for the differences seen in open circuit voltage and fill factors for the thin CdS cases. Presumably the resistive top layer and possibly the smoother texture of the USF TCO are responsible for these effects. Again it should be noted that our sputtering process has been optimized with LOF superstrates and the performances shown above and in Section 3.1 probably do not represent the best that can be achieved with an "all-rf-sputtered" cell on 7059 glass.

4.0 Studies of CdS_xTe_{1-x} alloys and CdS/CdTe interdiffusion: Raman, RBS, and GIXS

The heterojunction interface between CdS and CdTe is critical to the performance of the CdS/CdTe solar cell. It is known that interdiffusion occurs during the annealing after $CdCl_2$ treatment[8,9] and possibly some interdiffusion also occurs during growth, depending on the growth temperature. It is also generally accepted that some interdiffusion is necessary for obtaining a high efficiency CdS/CdTe solar cell. Although there have been some limited studies of the nature of the ternary alloy material, CdS_xTe_{1-x}, it is relatively poorly understood. Previous studies have examined the lattice constant and optical absorption of thin films produced by co-evaporation.[12] We believe that it is important to examine the nature of these alloy films produced under conditions similar to those used in the fabrication of a solar cell.

Three types of studies were performed to examine the alloy material and its formation. In Section 4.1 we describe the results of a study of a broad range of CdS_xTe_{1-x} alloy films grown by pulsed laser deposition. The preparation of these films was begun during the last contract year but was completed just recently. We present below a study of Raman scattering to determine the optical phonon frequencies. In the second part, below, we present some additional results from RBS studies of the interdiffusion between CdS and CdTe layers in bilayer films deposited on quartz glass. In the third sub-section, below, we present the results of an initial feasibility study of grazing incidence x-ray scattering (GIXS) to test the possibility of using GIXS as a measure of interface roughening between CdS and CdTe.

4.1 Raman scattering in CdS_xTe_{1-x} films grown by laser physical vapor deposition

Although most of our present solar cell fabrication effort is focussed on rf sputtered films, we have found previously that the films produced by LPVD are very similar to those produced by rf sputtering. For example, similar superstrate temperatures are used and similar growth rates are obtained. LPVD has the advantage that we can readily prepare a series of targets from mixtures of the binary compounds, CdS and CdTe, which will yield a broad range of alloy films.[13] We fabricate these targets by cold pressing from the mixtures with a standard hand-operated press at ~10 tons/in^2 (~10^8 Pa).

In the discussion below, which is largely taken from a manuscript recently accepted for publication in Applied Physics Letters,[14] we emphasize the analysis of the Brillouin-Zone-center longitudinal optical phonon frequencies across the full range of the alloy compositions. With the LPVD film growth, we found only a small gap in x-values near the middle of the alloy range, for $0.48 \leq x \leq 0.71$. The data are fit with an elementary lattice dynamics model which assumes that the anion sites, S and Te, are occupied by an average composition in proportion to the x-value.

We studied thin films prepared by a nonequilibrium growth technique, pulsed laser deposition (PLD), which cover the full alloy range. The Raman data are fit with a calculation of zone-center frequencies based on the modified random-element-isodisplacement (MREI) model.[15] To our knowledge, the only previous study of the alloy vibrational modes was done by Mityagin, et al.[16] on bulk CdS_xTe_{1-x} alloys quenched from high temperature. This study employed mainly infrared reflectivity and some limited Raman scattering at 1064 nm and was not accompanied by model calculations.

Ternary semiconductor systems show in general three different characteristics for the zone-center longitudinal optical (LO) and transverse optical (TO) phonons. These are identified as "single-mode", "two-mode", and "intermediate-mode" behavior. The origin of a particular behavior depends on the frequency of the impurity local vibrational mode relative to those of the LO or TO modes of the host lattice. An example of single-mode behavior is the $ZnSe_xTe_{1-x}$ system[13] where a single LO and TO branch is observed for every value of x. Typically in the alloys exhibiting single-mode behavior, the frequency of the impurity vibrational mode lies very close to the LO and TO frequencies of the host crystal for both binary end points, *i.e.*, Se in ZnTe and Te in ZnSe. $Cd_{1-x}Zn_xTe$ exhibits two-mode behavior.[17,18] In this case both CdTe-like and ZnTe-like LO and TO modes are observed. The optical phonon bands of the end points do not intersect and the frequencies of the local modes (Zn in CdTe and Cd in ZnTe) lie well outside the restrahlen region of the host crystals. For intermediate-mode behavior $Cd_{1-x}Zn_xSe$[19,20] is a good example; in this case the impurity mode lies between the LO and TO bands of the host crystal for both binary points and evolves as an intermediate band between the LO and TO branches.

Our data show that the CdS_xTe_{1-x} lattice dynamics have the two-mode behavior.

Table 4.1: CdS_xTe_{1-x} Films Prepared by PLD on Glass

Sample ID	CST20	CST22	CST23	CST4	CST5	CST1	CST2	CST3	CST17	CST16
target x	1	0.9999	0.99	0.97	0.94	0.90	0.80	0.70	0.60	0.60
film x-WDS				0.96	0.90	0.90	0.75	0.71	0.48	0.44
Sample ID	CST12	CST8	CST14	CST13	CST9	CST7	CST6	CST10	CTO15	
target x	0.60	0.50	0.50	0.40	0.20	0.10	0.050	0.020	0.000	
film x-WDS	0.41	0.29	0.28	0.20	0.11	0.057	0.031	0.017		

Nineteen different CdS_xTe_{1-x} alloy film compositions were grown by PLD on borosilicate glass. See Table 4.1. The samples were deposited at $5x10^{-6}$ Torr using an XeCl excimer laser (λ=308 nm with 80 mJ pulses at 20 Hz) as described previously.[21] The growth rate was ~0.5nm/sec.

All films were deposited at a substrate temperature of 360 °C except for CST 16 and CST17 which were grown at 275 °C and 200 °C, respectively. The lower substrate temperatures were chosen to try to increase the S sticking coefficient and the x-value of the film. In fact, as can be seen from the three films grown from the same 60% CdS target (CS12, CS16, and CS17) the sulfur content in the film increases from 41% to 48% as the growth temperature is reduced from 360°C to 200 °C. For most of the films, the composition was measured by wavelength dispersive x-ray spectroscopy (WDS) by Alice Mason at NREL and shows generally some depletion of sulfur in the films relative to the original target mixture. The sulfur depletion is greatest in the middle of the miscibility gap from about $0.7 < x < 0.1$. Except for the middle of the alloy range, the films are strongly oriented with <111> or <002> crystallographic texture.

The Stokes shift of the first-order longitudinal optical phonons for the CdS-like and CdTe-like modes were measured with a triple monochromator and CCD detector using a cylindrical focus and exciting wavelengths close to resonance with the direct optical gaps in the alloys. Because of the strong band bowing,[21,22] all of the alloy films with $x \leq 0.7$ lie close to resonance with the Kr^+-laser line at 752.5 nm. For the sulfur-rich films with $x > 0.7$, the 514.5 nm Ar^+ or 632.8 nm HeNe laser lines were used. All Raman studies were performed with the films at a temperature of about 10 K and laser power densities between 1 and 2 W/cm^2.

Figure 4.1 shows a set of Raman spectra measured in the backscattering geometry. The higher frequency peak corresponds to the CdS-like LO mode (LO_2) and the lower frequency is the CdTe-like LO mode (LO_1). The TO modes are much weaker and are not observed in most films since they do not undergo the strong resonant enhancement due to the Fröhlich coupling as do the LO modes. We note that both the CdS-like and CdTe-like modes have asymmetries toward lower frequencies which we attribute to alloy broadening.[23] This low-energy tail obscures the much weaker TO modes in most of our samples.

The LO Raman frequencies vs. sulfur concentration (x-value) for all samples are shown in Fig. 4.2. For lower x-concentrations the CdS-like LO_2 and TO_2 phonons should converge to the triply degenerate vibrational local mode of S in CdTe at 259 cm^{-1}. For $x \approx 1$ the CdTe-like LO_1 mode extrapolates to 162 cm^{-1} as observed from Fig. 4.2. Note that the CdS-like LO mode frequency increases substantially with sulfur concentration, whereas the CdTe-like LO mode decreases, but only slightly.

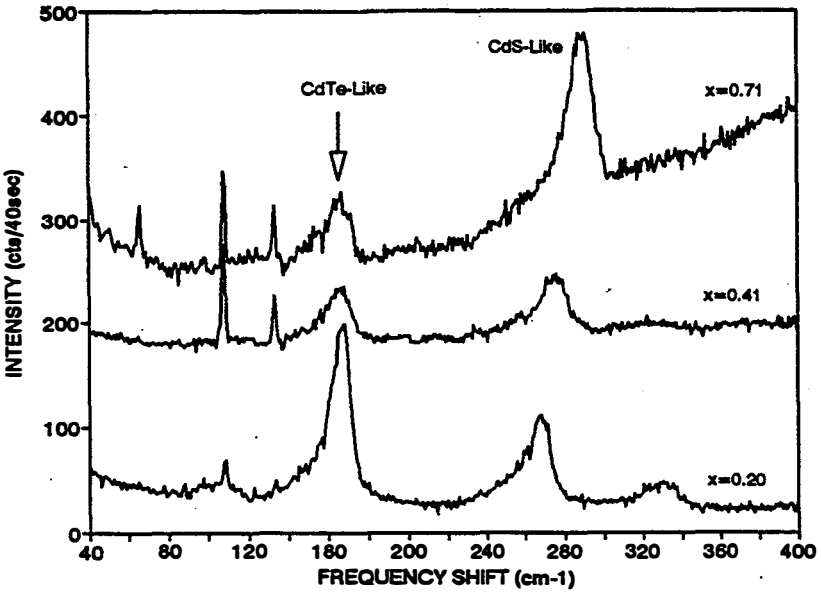

Fig. 4.1. Three Raman spectra taken at 10K from three pulsed laser deposited alloy films of CdS_xTe_{1-x}. x-values are shown. Note the asymmetry which results from alloy broadening effects.

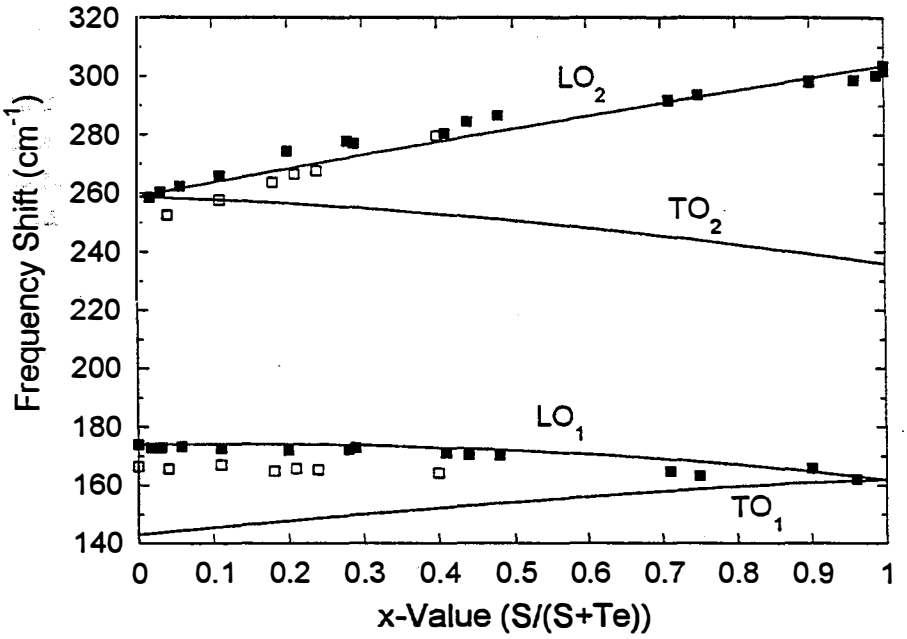

Fig. 4.2. Raman frequencies for all alloy films. Upper branch is the CdS-like LO mode and the lower branch is the CdTe-like LO mode. Solid lines are the results of the MREI model calculation of the zone-center phonon frequencies.

The solid lines in Fig. 4.2 represent phonon frequencies calculated according to the modified random element iso-displacement (MREI) model. A complete description of this model has been given elsewhere.[15,20] The most relevant assumptions in the MREI model applied to CdS_xTe_{1-x} are: first, the existence of two sublattices, one consisting of Cd atoms only, and the other consisting of S and Te atoms in a random arrangement. There is no short-range order imposed on the distribution of chemical species in this second sublattice. The second assumption of the model is that the anions (S and Te) and cations (Cd) each vibrate with the same phase and amplitude, *i.e.*, relative motions occur only between atoms of different chemical species. The random condition assumes that each atom is subjected to forces that are the statistical averages of interactions with their close neighbors.

We note good agreement between the experimental data and the fitted curves as seen in Fig. 4.2. Details of the fitting parameters--the two dynamic ionic charges and the three force constants are given in Ref. 14. However, the fit is systematically lower than the data in the LO_2 branch for $0.2 < x < 0.7$. Some shift due to differential thermal strain may be present in our polycrystalline films, but we expect this to be small. We have determined that for the films in the middle of the alloy range, $0.1 \leq x \leq 0.9$, there is substantial alloy broadening of the Raman lines. This has the effect of lowering the frequency of the observed Raman peak by 3 to 4 wavenumbers from the Brillouin-zone-center phonon frequency of the ideal crystal.

In summary, we have measured the longitudinal optic phonon frequencies in thin films of the CdS_xTe_{1-x} ternary compound by Raman scattering over the full alloy range. CdS-like and CdTe-like LO phonon branches are clearly observed as a function of relative anionic x-composition showing a "two-mode" behavior for this system. The CdS-like LO_2 mode has a large softening towards the CdTe binary end point, whereas a small softening is shown for the CdTe-like LO_1 mode towards the CdS binary end point. The application of the MREI-model to the fitting of our experimental points yields the force constants between all the atomic species, *i.e.*, Cd-S, Cd-Te, and S-Te. We have neglected in our calculations the anisotropy in the local electric field for the hexagonal phase; this is justified because the lack of detection of a splitting in the optical branches for the S-rich region and also because the local order is very similar in both structures. Except for slight underestimates of the LO frequency for $0.2 < x < 0.7$, the model fits the data well assuming a zincblende phase throughout. Moreover, the good fit implies that the S and Te atoms are indeed distributed in a random fashion in the anionic sublattice.

As a result of the extensive study of alloy films described above, it is now possible to use Raman scattering to determine sulfur composition (x-value) and thus to examine the characteristics of the interdiffusion in completed solar cells and in cell-type structures. For example, one may use Raman scattering either probing from the CdTe side or, with red laser light, probing through the glass, SnO_2, and the pure CdS.

4.2 RBS measurements of CdS/CdTe interdiffusion in thin bilayers

Regions of ternary alloy material are normally produced by interdiffusion in CdS/CdTe solar cells during the post-deposition annealing. In order to study this interdiffusion process, we prepared thin bilayer films for analysis by Rutherford backscattering. He^+ RBS at 1.52 MeV can conveniently probe CdS and CdTe layers of a total thickness of 200 to 300 nm. Because of the energy loss of the He ion as it passes through the solid, the backscattered energy of the He provides excellent depth resolution. In addition the kinematics of the backscattering process allows one to resolve elements with different masses.

At the 25th IEEE Photovoltaic Specialists Conference-1996 we introduced the first results of Rutherford Backscattering on CdS/CdTe solar-cell type structures.[24] Because sulfur is light compared to cadmium and tellurium, it appears well isolated from other elements if the layers are thin. However, due to the interference of heavy elements in soda-lime and in borosilicate glasses, it is necessary to use pure silica substrates. Figure 4.3 illustrates the type of RBS spectra which can be obtained from as-deposited layers on silica.

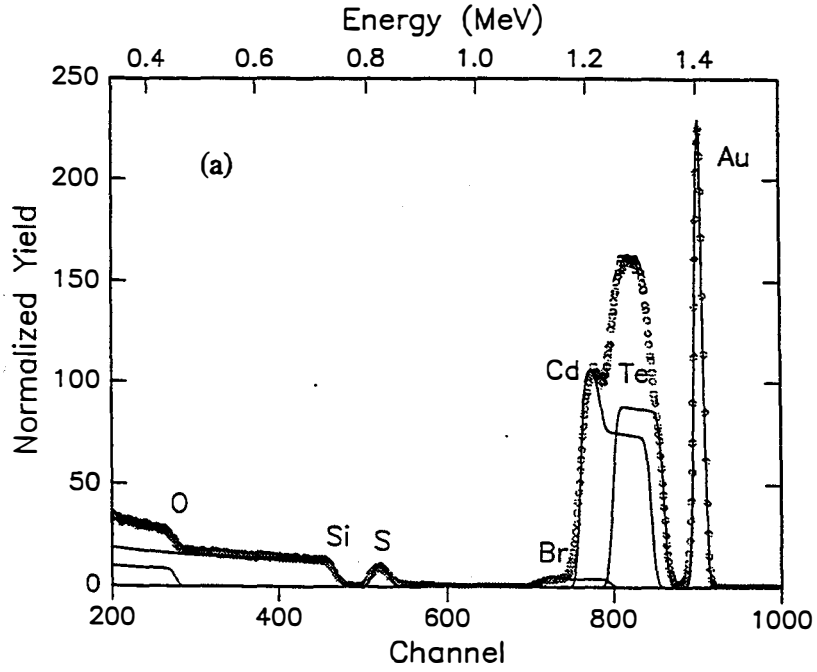

Fig. 4.3. Rutherford backscattering spectrum obtained by Mark Stan at CWRU with 1.53 MeV He^+ from as-deposited bilayer structure: 7 nm Au / 100 nm CdTe / 50 nm CdS / SiO_2. The sample was etched with Br:MeOH and residual Br at about the 5% level appears throughout the CdTe and CdS layers.

In this case the bilayer structure was etched briefly with a very weak Br:MeOH solution, following the same procedure as for the $CdCl_2$-treated and annealed samples described below. To avoid charging problems during RBS, the sample was coated with 7 nm of gold prior to

analysis. The gray points in the figure are experimental data, the solid curve is a RUMP[25] simulation of the He^+ backscattered spectrum. Although the sample was extensively rinsed in clean MeOH, a relatively strong Br signal appears under both the CdS and CdTe at a relative intensity of about 5%!

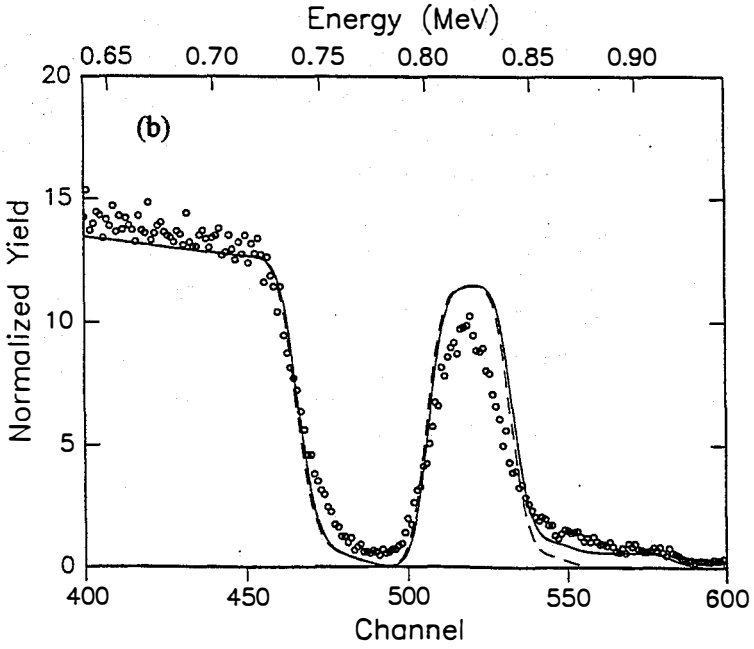

Fig. 4.4. Low energy section of RBS spectrum from bilayer film after $CdCl_2$ treatment and anneal at 385 C for 20 min. Sulfur peak shows a tail to higher energies due to diffusion into the CdTe. Dashed curve shows RUMP simulation with no S diffusion; solid curve - simulation with diffusion.

Our objective in this study was to examine the interdiffusion of the sulfur across the CdS/CdTe interface. Thus additional samples were treated with $CdCl_2$ in the usual way[1,26] and annealed in air for 20 minutes. The results from a sample annealed at 385°C for 20 minutes is shown in Fig. 4.4. This spectrum shows only the low energy region near the sulfur peak. In comparison with the as-deposited sample, the S peak shows a distinct tail extending to higher energies. This is caused by S diffusing toward the surface into the CdTe or along grain boundaries. We have used the RUMP simulation package to model this diffusion with a complementary error function form. In the figure the dashed curve is the simulation without diffusion; the solid curve is the simulated spectrum after diffusion with a diffusion coefficient of $D \cong 10^{-14}$ cm^2/sec. Similar results for the diffusion coefficient were estimated from photoluminescence studies.

Additional work with both RBS, Raman and photoluminescence is in progress to elucidate the interdiffusion mechanisms further.

4.3. Grazing incidence x-ray (GIXS) measurements of interface roughness

Interdiffusion at the CdS/CdTe interface is likely to proceed more rapidly along grain boundaries than inside the individual grains. If this occurs, there should be some roughening of the interface. In an attempt to examine interface roughness, we have collaborated with the group of Y.H. Kao of the University at Buffalo (SUNY). We supplied specially grown films of cell-type structures, CdTe/CdS/7059 glass, and inverted cell-type structures, CdS/CdTe/7059 glass. We chose to deposit directly on 7059 glass rather than SnO_2-coated glass in order to have the smoothest possible starting surface. The work done in the past year has been preliminary in an attempt to determine the feasibility of and the limits of the technique. Measurements were performed at the National Synchrotron Light Source at the Brookhaven National Lab by Frank Huang and Jack Soo. The basic ideas and some initial results are described below.

The basic experimental setup is sketched in Fig. 4.5, showing the Si(111) double crystal monochromator, defining slits, and the ionization chamber used for the beam fluence monitor. At the sample position is a Li-drifted silicon (SiLi) x-ray fluorescence detector, and the BICRON detector is used for the scattered beam detection. At a photon energy of ~30 keV, the index of refraction of CdS and CdTe is slightly less than unity and thus, near grazing incidence the x-ray beam will undergo total *external* reflection. (Analogous to total internal reflection of light at the core-sheath interface of an optical fiber.) For angles of incidence below the critical angle, θ_c, the penetration of the evanescent is strongly attenuated. Consequently the probe depth can be angle tuned. The inverted solar cell structure (with the CdTe on the bottom) was convenient for testing the evanescent wave penetration. Figure 4.6 shows a series of x-ray fluorescence spectra taken as a function of the angle of incidence (the angle between the propagation vector of the incident x-rays and the parallel to the surface). Note that the Te K_α peak disappears near an incident angle of θ=0.06° at which point the x-ray beam does not penetrate beyond the 250 Å thickness of the CdS layer.

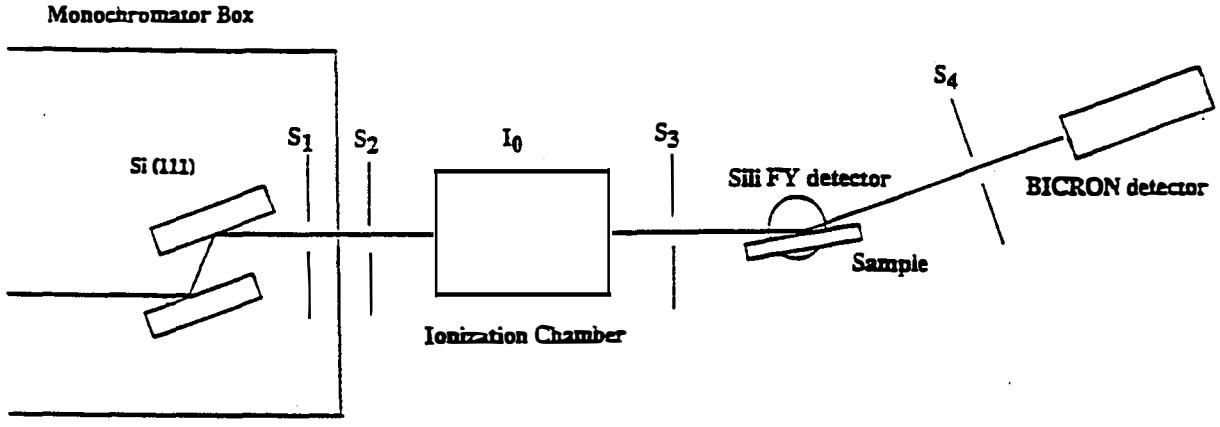

Fig. 4.5. Experimental setup for for grazing incidence x-ray measurements at the Brookhaven NSLS synchrotron beam line X3B1. Thin CdS/CdTe bilayers are placed at the sample position with x-ray fluorescence detection by a Si:Li detector and reflected beam detection with the BICRON detector.

Fig. 4.7 gives a summary of the analysis of the Te fluorescence data giving the 1/e penetration depth of the 31.9 keV x-rays as a function of the angle of incidence. Note that the critical angle is θ_c = 0.075°.

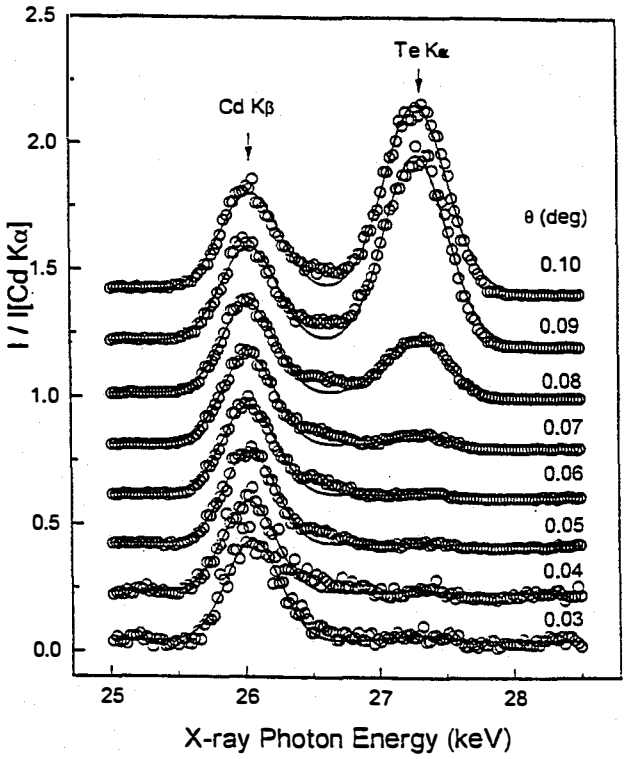

Fig. 4.6. X-ray fluorescence from S and Te obtained with a grazing incidence 34 keV synchrotron x-ray beam from a bilayer structure CdS/CdTe/glass.

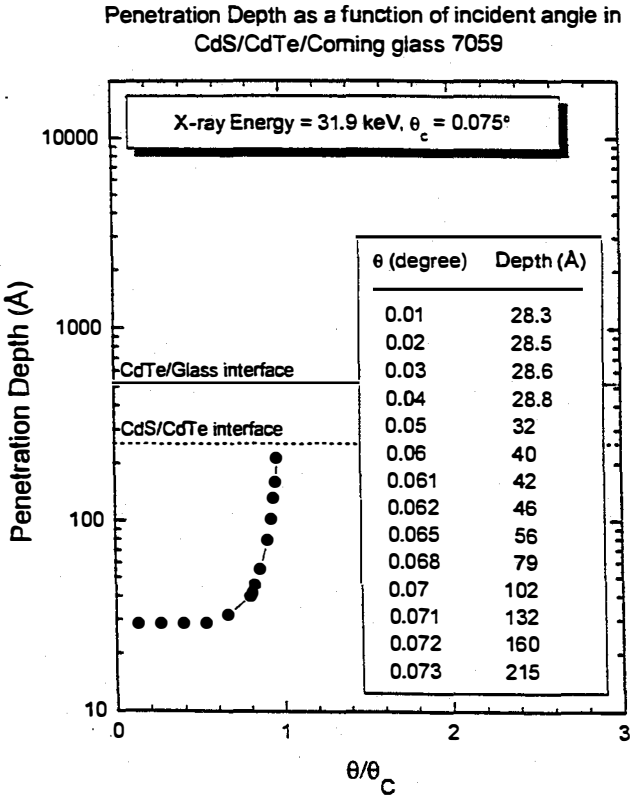

Fig. 4.7. x-ray 1/e penetration depth as inferred from the Te x-ray signals of Fig. 4.6.

Interface roughness is measured by the specular reflection of the x-ray beam and the amount of interference which arises from front and back interfaces. This is shown for the case of individual films of CdS and CdTe on glass in Fig. 4.8. Note that for the reflectivity the periodicity of the interference fringes allows one to obtain directly the film thickness. The amplitude of the interference fringes yields the surface and interface roughness. The results for these single films are given in the inset of the figure. For the more complicated bilayer structures the reflectivity results are given in Fig. 4.9. In this case modeling of the structures allows one to obtain the thickness of each film as well as the roughness of the surface and interfaces. All of the above results were obtained on as-deposited film grown by rf sputtering at 380 °C.

This initial study confirms that the GIXS technique[27] is readily applied to rf sputtered films as long

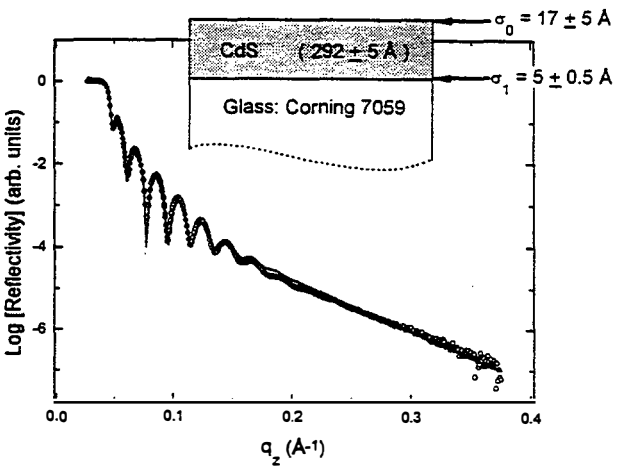

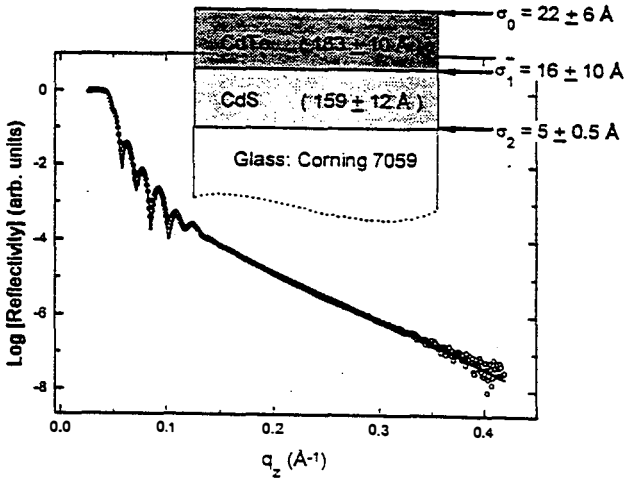

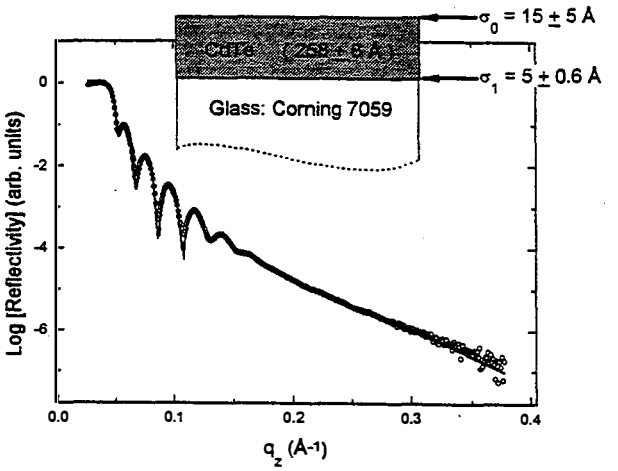

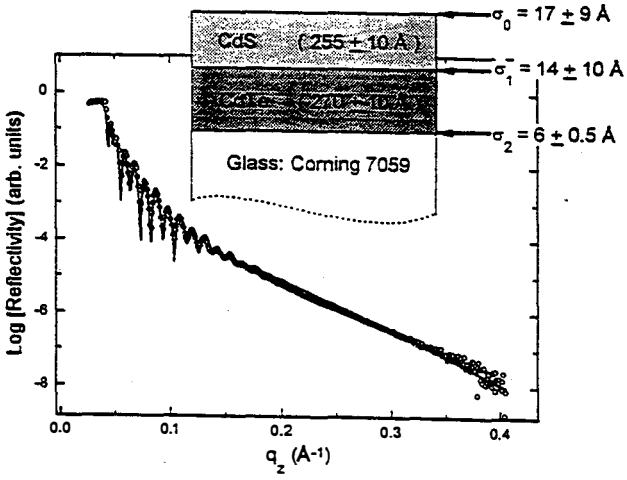

Fig. 4.8. Experimental reflectivity (circles) and calculations (lines) for single CdS and CdTe films on glass. Thickness and roughness are inferred from the fit.

Fig. 4.9. x-ray reflectivity data (circles) of a bilayer structure on glass. Thicknesses and roughness parameters inferred from the fits (lines) are indicated in the figure.

as they are appropriately thin (~200 Å). Further experiments are now in progress with films which have been treated with $CdCl_2$ and annealed to try to quantify additional interface roughening as a consequence of interdiffusion.

5.0 Admittance Spectroscopy on rf sputtered CdTe cells

In last year's annual report, we mentioned that there was ongoing work in our group in capacitance-voltage measurements on cell structures. Near the end of the current phase, Eugene Bykov completed his M.S. thesis work[28] and some of the results of his studies will be described here. He found that the capacitance and its voltage dependence could vary substantially from contact to contact (4 mm diameter) over the ~35 cm^2 sputtered film area. Thus the results reported here should be regarded as tentative, at best.

5.1 Instrumentation

The admittance spectroscopy system was constructed around a Stanford Research model SR-510 lock-in as outlined in Fig. 5.1 below. The excitation signal was derived from the voltage controlled oscillator of the lock-in through an A/D port of the lock-in. The signal current was converted to a voltage signal through a transimpedance amplifier constructed from a high speed, low noise operational amplifier (TLE2071). The ac excitation signal of typically 3 mV and the dc bias were mixed in a buffer amplifier. For calibration purposes, at each new frequency, the computer-controlled (via a PCL-812 interface card) relay switched in a fixed, pure resistor in place of the sample. Control of the lock-in and data acquisition were accomplished by the RS232C communication port. Capacitance-voltage and capacitance-frequency measurements were made at, as well as slightly above and below, room temperature.

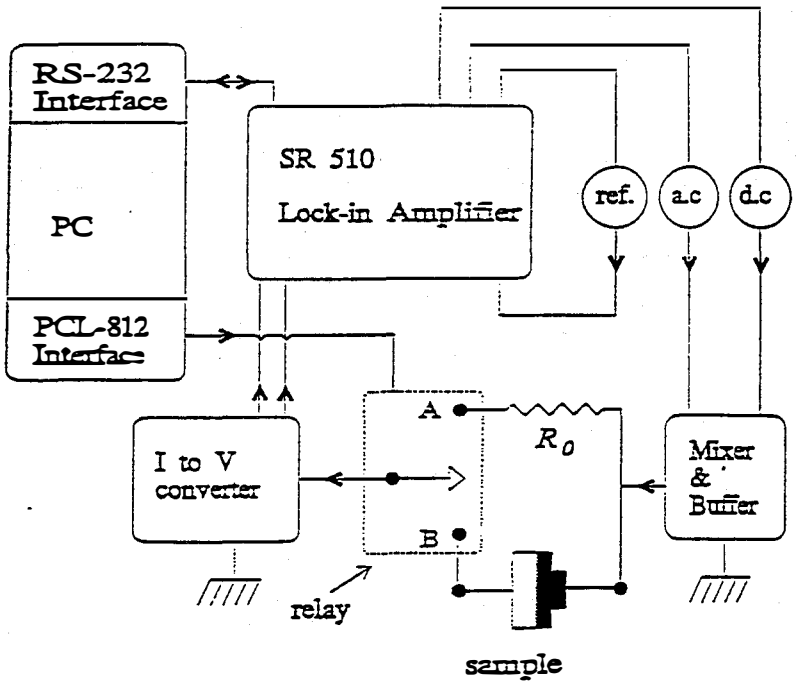

Fig. 5.1. Instrumentation for the admittance spectroscopy measurements.

5.2 Schottky contacts on CdS and CdTe films

Schottky barriers were formed with evaporated gold contacts on rf sputtered CdS on LOF SnO2:F-coated glass. Fig. 5.2 shows the $1/C^2$ vs V plots for three contacts on an as-deposited film and one contact formed on an adjacent area after $CdCl_2$ treatment and anneal for 20 min at 385 C. The response after treatment indicates a considerable reduction in the density of donors and trap states from 30-60 x $10^{15}/cm^3$ in the as-deposited film to 13 x $10^{15}/cm^3$ in the film after the $CdCl_2$ treatment and anneal. Under some growth conditions, such as when sputtering is done with some substrate bias or if small amounts of oxygen are used in the sputter gas, it is not possible to form a good Schottky barrier unless the $CdCl_2$ treatment is used. If good Schottky barriers can be formed with evaporated gold on the as-grown film, we interpret that as indicating a dense film which permits little diffusion of gold along grain boundaries and relatively few intragrain defects which might enhance the gold diffusion. The $CdCl_2$ treatment step apparently removes some of these problems in films grown under poor conditions.

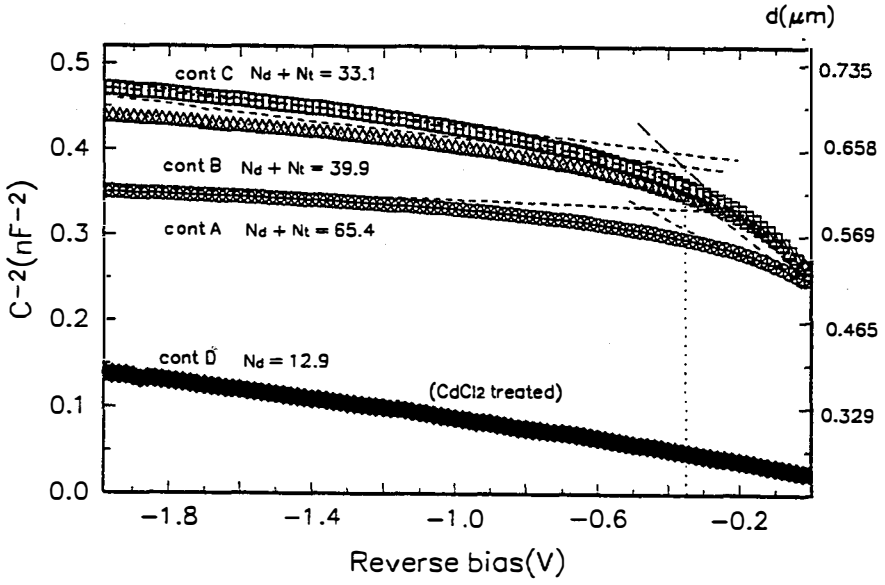

Fig. 5.2. $1/C^2$ vs. bias voltage for several 4mm diameter evaporated gold contacts on sputtered CdS on LOF glass. (CS116). f=100 kHz. Contacts A,B, &C were on an as-deposited film. Contact D was on the same film after $CdCl_2$ treatment and 385 °C anneal for 20 minutes in air.

Schottky barriers formed with CdTe sputtered directly on the LOF SnO_2:F performed quite well and showed little sensitivity to the CdTe sputtering conditions. The standard $CdCl_2$ treatment process tended to decrease slightly the hole concentration so that the entire film thickness of up to 2 μm was depleted.

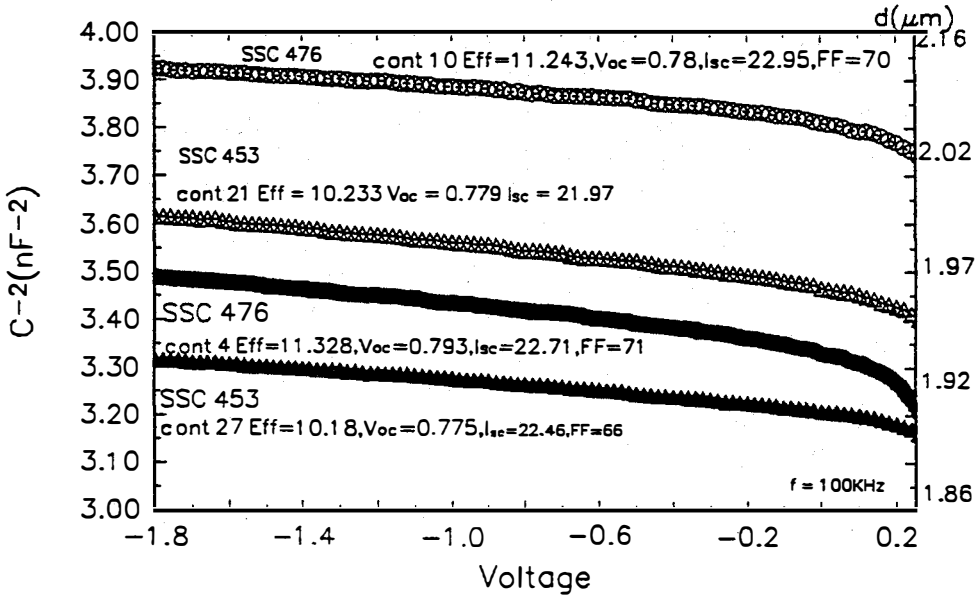

Fig. 5.3. $1/C^2$ vs. bias voltage for two contacts on each of two different rf sputtered cells. Film SSC453 was sputtered in pure Ar; film SSC476 was sputtered in ~1% O_2 in Ar.

5.3 Admittance measurements on cells

Admittance measurements were also made on some of our standard rf sputtered cells on LOF glass superstrates. Fig. 5.3 shows a plot of the $1/C^2$ vs V curves for two contacts on each of two different sputtered film growths. One film was sputtered with pure argon (SSC453) and the other film was sputtered with the addition of ~1% O_2 to the argon. First, it can be noted that the variation of the capacitance varies as much from contact to contact on the same film as between the two films. In addition, note that the capacitance shows only a small dependence on bias voltage. This suggests the presence of an intrinsic layer with a capacitance which is nearly independent of the bias. If the reciprocal of this intrinsic layer capacitance is subtracted from the reciprocal of the measured capacitance, the inverse reciprocal squared of this remaining capacitance, plotted in Fig. 5.4 vs. bias, is consistent with an almost uniformly doped semiconductor. For the four contacts studied, the acceptor concentration inferred from these measurements ranges from 5 to 12 x $10^{17}/cm^3$. Note that the cell efficiencies ranged from 10.18% to 11.3% so that these acceptor concentrations appear to correlate poorly with the cell performance. In fact, the values of the intrinsic capacitance ranged from 0.52 nF to 0.56 nF which imply an intrinsic layer thickness, for these 4 mm diameter contacts, of ~2 μm or very nearly the full CdTe thickness. Thus the voltage-dependent capacitance probably arises from the doped layer near the back contact, which may be due to the in-diffusion of the 4 nm layer of evaporated copper deposited before the 25 nm layer of gold. (Note that the cell received a 30 min heat treatment at 150°C after the metallization.) The C-V measurement seems to be picking out this doped layer near the back junction. These data imply that C-V measurements could be used to study this back contact diffusion, although if the CdTe is thicker than 2 μm, the subtraction is

unreliable.

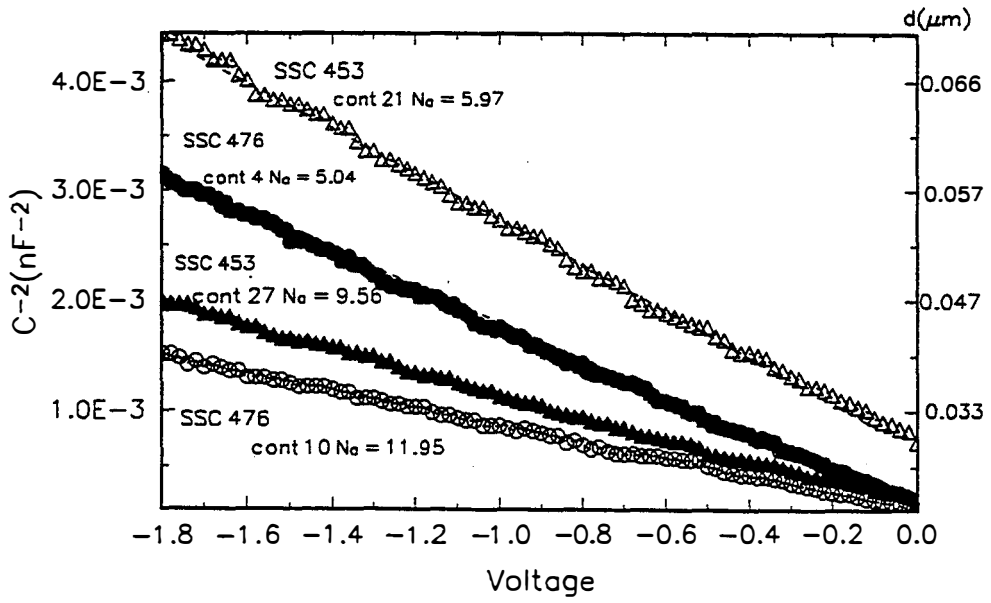

Fig. 5.4. $1/C^2$ vs. V curves after subtracting the effect of an intrinsic layer capacitance. Cells (contacts) are SSC453 contacts 21 and 27 and SSC476 contacts 4 and 10. The subtracted values of the intrinsic capacitance, C_i, were, respectively 0.545, 0.563, 0.555, and 0.515 nF.

5.4 Frequency dependence of the admittance

Additional studies were made of the frequency dependence of the capacitance in these p-i-n junction cells made by rf sputtering. Frequency-dependence measurements were made in three different ways--as a function of temperature, as a function of bias, and as a function of cell efficiency. Here we present results for the bias dependence and the efficiency dependence.

Figure 5.5 illustrates the frequency dependence of the capacitance for three dc biases. In reverse bias (V_b=-1V) or zero bias, there is little change in capacitance with frequency. However, at a forward bias of 0.3V there is a substantial increase in capacitance at low frequencies, below about 300 Hz. These data were taken from a cell which had an efficiency of about 9.5%.

To test for correlation between the cell efficiency and the frequency dependence, we tested five different contacts on one film. These contacts (cells) had efficiencies ranging from 7.5% to 11.3%. The frequency dependence is shown in Fig. 5.6. The data of Fig. 5.6 indicate a strong correlation between the cell efficiency and the density of extraneous states with long time constants. Thus the two cells with efficiencies over 11% show the lowest dispersion, and the cells with efficiencies of 10.2%, 9.4% and 7.5% have increasing dispersion. The cell with efficiency of 7.5% has particularly strong increase in capacitance at low frequencies.

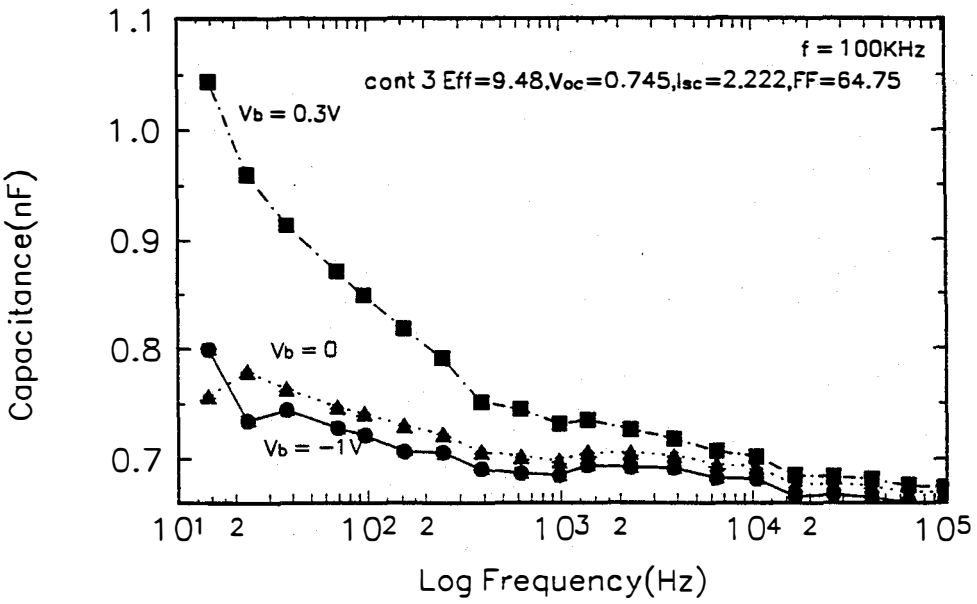

Fig. 5.5. Frequency dependence of the capacitance for three dc biases on contact 3 of cell SSC424.

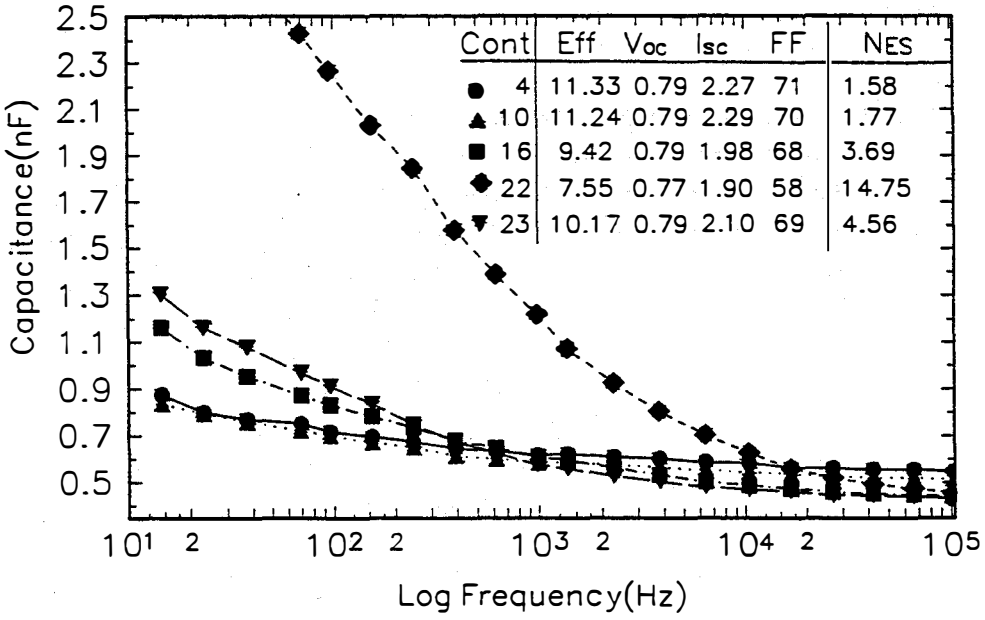

Fig. 5.6. Correspondence between frequency dependence of the capacitance and cell performance for five cells on a single rf sputtered film.

6.0 CdS Photoluminescence--Dependence on Magnetron Magnetic Field

In earlier reports we have described a strong dependence of sputtered solar cell performance on the magnetic field of the planar magnetron. For example we found that when a strongly unbalanced magnetron is replaced by a nearly balanced field magnetron for the deposition of the CdTe layer, the cell performance dropped from about 11% to ~3% even though all the other deposition parameters and post-deposition cell processing were kept constant. In this test, the unbalanced magnetron was from AJA International and the balanced field magnetron was from KJL. In addition to the configuration of the magnetic field, the construction of the two guns were different, with modular magnets used by AJA for the outer ring and an annular magnet used by KJL. The field strength just above the target surface was much less for the KJL gun as well. In order to try to identify more directly the effects of the magnetron magnetic field (strength and structure), we deposited several pure CdS films on 7059 glass and on LOF/SnO_2:F glass. Films were prepared by sputtering i n pure Ar and in Ar with 1% O_2. We then examined these films by low temperature photoluminescence and by electrical conductivity, as well as Hall measurements where possible. The electrical studies were performed by one of the two summer NSF Research Experiences for Undergraduates students, Danielle Anderson. A description of her results is given in the Section 7.

In the figures below, photoluminescence data are shown from four CdS films rf sputtered onto NEG 0A-2 glass at 360 °C. Two films were grown in pure Ar and two were grown in the 1% O_2/AR mixture. To avoid complications from different gun designs, we used the AJA gun for two field configurations. The "39/3" configuration has been our standard with a stack of three NdFeB magnets in each of the 13 outer slots and a stack of three in the center. For the nearly balanced configuration, replacement magnets and slugs were obtained from AJA although these were longer so that the slots accomodated only a stack of two. Hence with the 13 outer slots filled with one magnet and one slug and with the center slot filled with two magnets of twice the diameter of the outer ones, we have the configuration "19.5/12" which we term a nearly balanced configuration. However the field strength for this gun with this "19.5/12" configuration is substantially greater than for the KJL gun. At the target surface the 19.5/12 configuration has an estimated tangent field of B≈ 500 G whereas the KJL gun has B= 50 G.[29]

Figure 6.1 displays the PL signal obtained at 10K with 2 mW of 458 nm excitation on 0.25 μm CdS grown with pure Ar as the sputtering gas. The two spectra are for films grown with the two different field configurations. Both spectra show a near band edge peak at 4900 Å and a broad peak at 6100 Å, the so-called R-band, which has been attributed to Cd vacancies in CdS. The one distinct difference is the presence of a peak at 5050 Å
magnetron. The origin of this peak is not yet known but it probably arises from a donor-acceptor pair recombination about 80 meV below the band-to-band transitions.

Figure 6.2 displays the PL signal from two films grown under similar conditions except that 1% O_2 was added to the sputter gas. In this case, there is no near-band-edge peak for the films grown with the nearly balanced gun and the near-band-edge (NBE) peak for the unbalanced gun is shifted lower by about 50 Å from that of the films grown without oxygen. The spectra are dominated by a strong,

narrow peak at 5050 Å. This peak may arise from oxygen dopants in the film, or also from possible damage to the film from bombardment with O^- ions which are known to be very stable. If these negative ions are formed by charge exchange at the sputter target surface, they would be accelerated across the cathode fall region to initial energies of about 100 V which is the target self-bias potential. Note that the deep level PL is weaker in these films grown with oxygen and the film grown with the unbalanced gun has noticeably less deep level PL than that grown with the nearly balanced gun.

Although these characteristics of the PL spectra are still open to some interpretation and are not clearly associated with particular types of defects, there is consistent evidence that the films sputtered with the unbalanced gun have stronger and cleaner NBE PL which is consistent with a higher quality film. Addditional evidence of the effects of the B-field configuration has been obtained in electrical measurements which are described in the next section.

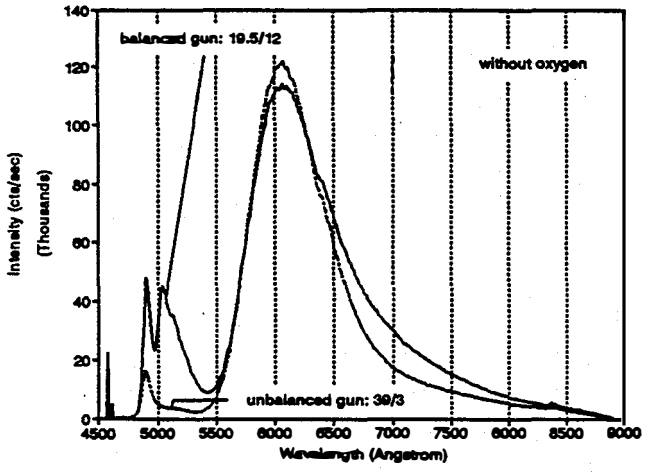

Fig. 6.1. 10K PL excited at 458 nm from CdS films grown with balanced and unbalanced magnetron fields.

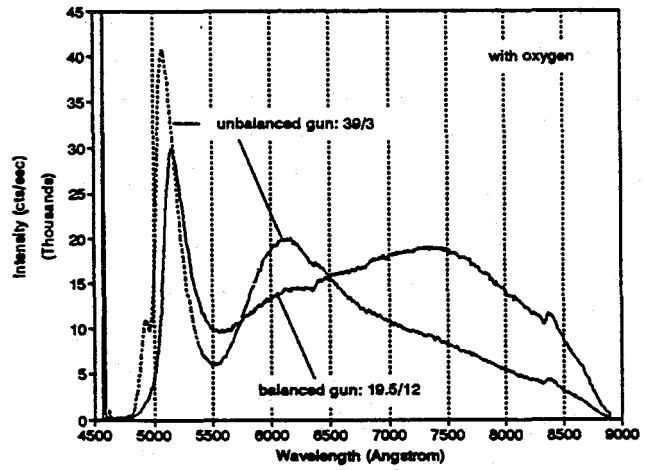

Fig. 6.2. 10K PL excited at 458 nm from two CdS films grown with balanced and unbalanced guns in 1% O_2.

7.0 Summer 1996 NSF Research Experiences for Undergraduates projects

Two undergaduate students were involved in this photovoltaic project during the summer of 1995 as part of the National Science Foundation's Research Experiences for Undergraduates Program (REU) at the University of Toledo Department of Physics and Astronomy. These students were Joe Britton and Danielle Anderson.

Joe Britton, who is an undergraduate physics major at the University of Chicago, worked on the analysis of the *in situ* optical transmission during CdS and CdTe film deposition to include the effects of interference. In most cases of interest to us, the final film thickness is large compared to the optical absorption length of the probing beam. (We had chosen 457.9 nm for the probe wavelength for CdS in order to satisfy this criterion.) However, in the course of working toward very thin layers of CdS, we recognize that we need to account for the interference effects in CdS since the 1/e absorption length is approximately $1/\alpha = 10^{-5}$ cm =100 nm. For example in the CdTe teaming activity, we have used thicknesses as low as 30 and 50 nm. In this work Joe, and a current undergraduate student, Dan Roach, produced the fit shown in Fig. 7.1 below. This represents the 457.9 nm transmission as a function of deposition time. We made the assumption that the growth rate was constant. The growth rate was calibrated by using a stylus profilometer trace across a scribe line made near the location of the probe beam. Interference effects are clearly visible as expected. However, the assumption of constant growth rate appears not to hold at the very beginning where there appears to be a delay of about 80 seconds in the onset of the normal growth rate. (The fitted curve starts with a shift of ~7 nm.) This appears to indicate the presence of a slow growth nucleation phase for growth on bare 7059 glass. We have not observed this for SnO_2-coated LOF glass.

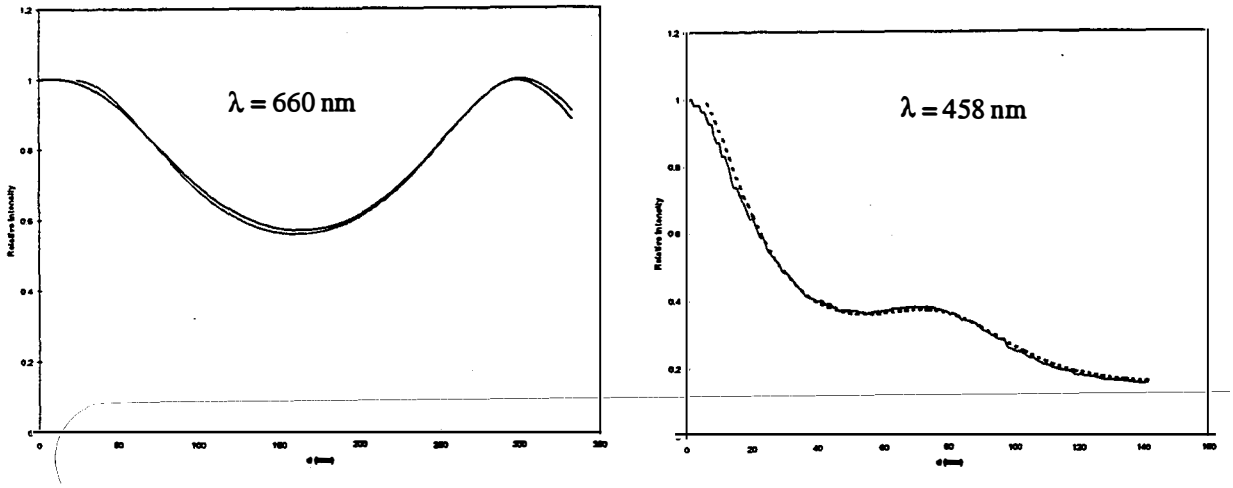

Fig. 7.1. Illustration of the fit obtained for the transmission of 458 nm and 660 nm light through a growing CdS film on glass. Interference effects are strong at 458 nm until the film thickness exceeds the absorption length, $1/\alpha \approx 100$ nm.

The second student, Danielle Anderson, is a student at the University of Toledo and during the summer worked with Randy Bohn. Danielle studied electrical properties of CdS films sputtered with different configurations of magnetic fields of the sputter guns. As noted in last year's annual report, we find major differences in cell performance depending on the magnetic field of the magnetron. However, since cell performance depends on a number of variables, such as those associated with deposition conditions of two semiconductor layers, the $CdCl_2$ treatment, and the contacting method, we decided to study the electrical properties of one of the semiconductor layers, CdS, as single films on borosilicate glass. Consequently, we prepared several CdS films on NEG 0A2 and Corning 7059 glass with three types of magnetron magnetic field configurations.

Using the AJA International gun with its modular magnets, we deposited films with magnet configurations of "39/0", "39/3", and "19.5/12". As shown in Fig. 7.2 this planar magnetron has an outer ring of 13 magnet columns and a central magnet column. Each of the outer columns can accomodate a stack of three 3/8 inch diameter NdFeB magnets or a maximum of 39 magnets in the outer ring. If the inner column has a similar stack of three 3/8 inch magnets the configuration is termed "39/3". This is our standard configuration. However, the field can be configured to be more unbalanced by replacing the center stack by a set of ferromagnetic slugs (0 magnets) to yield a "39/0" configuration. Alternatively, to reach a nearly balanced configuration, we replaced the center position with a stack of magnets of twice the diameter (equivalent to a stack of 12 3/8 inch magnets) and all the slots of the outer ring were filled with one ferromagnetic slug and one NdFeB magnet with a length of 1.5 times the original magnets, or 13 x 1.5 = 19.5 magnets; hence the description, "19.5/12".

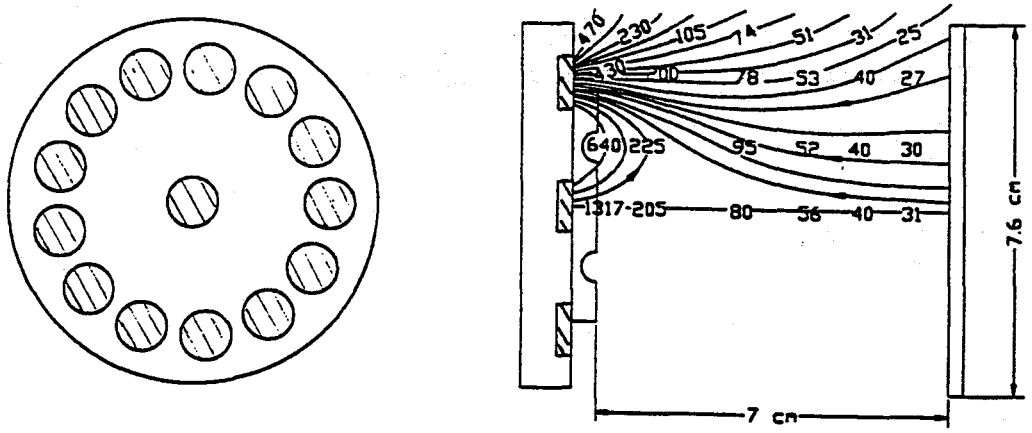

Fig. 7.2. Sketch of AJA International sputter gun with modular magnet arrangement. Field lines are sketched for the case of all 39 outer magnets in place and a stack of three 3/8 inch magnets in the center (39/3).

In addition to the three types of magnetron magnetic fields, CdS films were grown with and without a small amount of oxygen (~1 at. %) mixed into the Ar sputtering gas. The results of Danielle's conductivity studies are shown in Figure 7.3. These are measurements of the dark resistivity taken on films ~1 μm thick. For the films grown without O_2 the resistivity appears to go through a for the standard (39/3) field configuration. Remarkably, though, the situation with films grown in the presence of small amounts of oxygen is that the resistivity decreases monotonically as the field becomes more balanced. With the two unbalanced field configurations, the addition of 1% O_2 to the argon during sputtering increases the resistivity slightly. However, with the small amount of oxygen and the most balanced field configuration the effect of oxygen is dramatic. It lowers the dark resistivity by about a factor of ten! It is possible that some of these effects with oxygen in the sputter gas may arise from the formation of the oxygen negative ion, O^-, which is known to be quite stable, and bombardment of the substrate during growth. These interesting effects are presently being explored further by graduate students.

The lowest resistivity film (denoted as CS102) also exhibited time dependent effects which we attribute to persistent photoconductivity (PPC). Immediately after being placed in the dark at room temperature, the carrier density was 4.3 x 10^{13} /cm3 and the mobility around 10 cm^2/V-s. Over the next 120 minutes the resistivity changed and reached a steady-state value. Here the mobility was also 10 cm^2/V-s but the carrier density had decreased to 2.0 x 10^{13} /cm3. Thus, it seems that at least some of the traps are associated with macroscopic barriers[30] which lead to long recombination times after light exposure. In order to further confirm the equilibrium values for the mobility and carrier density, CS102 was placed in the dark for 9 days at room temperature and remeasured. The results were confirmed to within the experimental uncertainty (approx. 6%).

Activation energies were also determined in the vicinity of room temperature by making Hall measurements between 270 K and 330 K for CS102 after it had been in the dark for 9 days. The activation energies for the conductivity, the carrier density, and the mobility were 0.23 eV, 0.16 eV, and 0.072 eV, respectively. If the activation energy for the mobility can be associated with the barrier height between grains, then a comparison can be made with the value obtained by Orton, et.al [31]. His value was 0.15 eV. In his model the barrier height does depend on the grain radius as r^2. Using a scanning tunneling microscope we determined that the average grain radius for CS102 was smaller than Orton's by a factor of about 0.69. Using this with Orton's model we find that the smaller barrier height is not unexpected and the agreement is quite good considering the approximations that have been made.

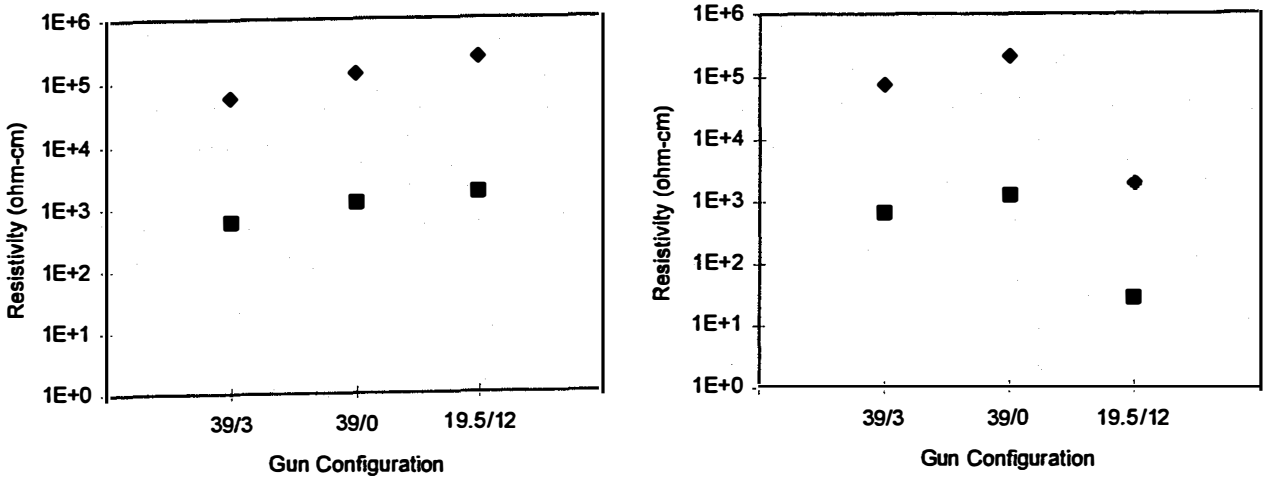

Fig. 7.3. Dark and light resistivity of CdS films sputtered with different magnetic field configurations as described in the text. a) films sputtered with pure Ar; b) films sputtered with 1% O_2 in Ar. ◆ = dark; ■ = AM1.5 resistivity.

8.0 Conclusions

Continuing our emphasis on rf sputtering for the CdS and CdTe deposition, we have shown that the sputtering rate can be increased at least to ~30 Å/sec with very little change in the materials quality. In order to achieve additional flexibility, particularly with respect to using thinner layers of CdS, we have instrumented a second sputtering system which has been used for deposition of intrinsic layers of SnO_2, as well as experimenting with the use of cold-pressed targets incorporating non-stoichiometric CdTe targets and trace elements of potential dopants. An additional system is being activated for dc sputtering of metals to provide additional fexibility in exploring the use of other metals for back contacts to the CdTe.

We participated in CdTe-teaming activity through the fabrication of rf sputtered cells on substrates supplied by Chris Ferekides (USF). In the two rounds of activity, we have now fabricated all-sputtered cells with CdS thicknesses of 300 nm, 200, 100, 60 nm (first round) and 80, 20, 0 nm (second round). In this activity, we have prepared cells side-by-side on the 7059/USF superstrates and on soda-lime glass/LOF superstrates. This work has shown very clearly the effect of the intrinsic SnO_2 layer on the USF. We have found that sputtered cells with no CdS have V_{OC} of 760 mV on USF superstrates but only 470 mV on LOF superstrates and each have fill factors of only about 56%.

Because the properties of the CdS/CdTe interfacial region are so critical to the performance of the CdTe solar cell, we have placed considerable emphasis on studies of the ternary alloy, CdS_xTe_{1-x}. We prepared by pulsed laser deposition an extensive collection of these films and then mapped the shift of the phonon Raman peaks as a function of the x-value. We found that this alloy exhibits two-

mode behavior with a CdTe-like LO_1 mode and a CdS-like LO_2. The CdS-like mode frequency increases with x-value and we have used this Raman peak as a marker to study the interface region in solar cell structures.

With our *in situ* optical thickness monitors and the related capability to deposit controllably very thin layers, we have fabricated several very thin layers and bilayers optimized for collaborative studies using Rutherford backscattering and grazing incidence x-ray reflection and scattering (GIXS). These studies are designed to provide quantitative data on interface interdiffusion and on interface and surface roughening. A preliminary estimate of interface interdiffusion from the RBS data indicate a diffusion coefficient at 370 C of $D \simeq 2x10^{-14}$ cm^2/sec. GIXS measurements of roughening of the interface after annealing are now in progress. Further collaborative work is in progress with IEC (Brian McCandless) for x-ray studies of the interdiffused layer and NREL (Dean Levi) on transient PL studies of the CdS_xTe_{1-x} alloys especially those with $x \approx 1$ and $x \approx 0$.

9.0 Future Directions

The cells we have fabricated by rf sputtering of the CdS and CdTe layers thus far have displayed two important limitations. The first is low short circuit current which is due to the relatively thick CdS layer (~0.2 μm). The second limitation is the relatively poor stability which is related to the diffused copper/gold back contact structure. Over the past year we have been building in-house capability to address and hopefully solve these issues for the case of our rf-sputtered cells.

Regarding the fabrication of cells with very thin, or no CdS layers, our participation with the CdTe team has shown that when intrinsic SnO_2 layers are used before the deposition of CdS, the cell performance is much better than without such i-SnO_2. Therefore, we have retrofitted an old sputtering chamber with an rf sputtering gun to use for deposition of such i-layers on LOF glass or other commercial substrates. We have optimized recently this rf deposition process and expect to place a major effort at systematically studying jointly the i-SnO_2/CdS thicknesses to achieve the highest possible J_{SC} while maintaining the highest possible V_{OC}. We have recently acquired a CdTe sputtering target with 4% CdS to use for cells prepared with thin or no CdS.

Addressing the issue of contact stability, in the past we have collaborated with IEC and with SCI to evaluate the suitability of other contacting schemes. Some results have been encouraging but we have found evidence that different CdTe growth processes require independently optimizing the contacting methods. For example, the post-deposition treatment and contacting conditions which work well for higher temperature vapor deposition of CdTe do not automatically work well for the lower temperature deposition of rf sputtering. During the past six months we have installed a dc sputtering system, donated from Harris Semiconductor, which we intend to use for studying other types of contacts. This system is now operational and a strong effort will be placed in the next year on evaluating other contacting schemes.

Contacting difficulties are aggravated by the problem of achieving heavy p-type doping of CdTe by atoms other than copper. However, it is hoped that the presence of the plasma present in rf

sputtering may allow for the possibility of enhancing the activation of other p-type dopants. We have recently started some efforts to use non-stoichiometric CdTe targets, together with reactive sputtering by small additions of N_2 to the Ar sputtering gas, to improve the activition of the nitrogen dopant in CdTe and ZnTe. We expect to continue this work, exploring other dopants as well.

In the topic of CdS/CdTe interface interdiffusion, we are presently completing studies of an extensive set of CdS_xTe_{1-x} alloy films deposited by pulsed laser deposition. We have completed the Raman studies and are finishing the optical absorption, x-ray diffraction, electrical conductivity, and photoluminescence. Some of these samples have been sent to NREL for additional studies using time resolved optical methods and high resolution microscopies. This effort on the alloy films should conclude in the next year.

Improved understanding of the alloys should help to sort out the details of the interdiffusion. In this regard, we are currently finishing a series of measurements using Rutherford backscattering and with photoluminescence on thinned cell structures to measure the diffusion rate of S into CdTe as a function of anneal temperature after $CdCl_2$ processing. We have obtained an estimate of the diffusion coefficient at ~370 C ($D \cong 2x10^{-14}$ cm^2/sec) and expect to measure the activation energy for this process, to help sort out the relative contributions of grain boundary vs. intra-grain diffusion. Also we have tested the potential for using grazing incidence x-ray reflection and scattering to measure the roughening of the CdS/CdTe interface. We expect to obtain some results for this roughening as a function of anneal temperature as well. This should provide information complementary to the RBS measurements.

Through these combined efforts in the next year we aim to improve our current best efficiency, for an all-rf sputtered cell, of 11.6% to reach well into the 13% range by the end of the next contract year. In addition, we shall continue appropriate participation in the CdTe teaming activities in both the thin-CdS team and the stability team.

10.0 Acknowledgments

Many individuals in addition to those at the University of Toledo have contributed in different ways to the work over the past year. At Solar Cells Inc., we thank Gary Dorer, R.C. Powell and Rick Sasala for helpful suggestions as well as some contacting studies. At IEC, we are indebted to Brian McCandless for contacting studies and further suggestions. For the CdTe Teaming activity we are indebted to Chris Ferekides of the University of South Florida for the 7059/TCO superstrates. For measurements on the completed cells we thank Jim Sites, Jennifer Granata, and Karl Schmidt of Colorado State University. At NREL, we are indebted to Alice Mason for WDS measurements on many alloy films, and to Dean Levi and Richard Ahrenkiel for time-resolved absorption and PL studies. For supply of superstrate material, we especially thank LOF and Peter Gerhardinger. We are especially grateful to our contract monitor, Bolko von Roedern, for helpful discussions and suggestions. Also at NREL we have benefitted from discussions with Pete Sheldon, Ramesh Dhere, Kannan Ramanathan, and Tim Gessert.

11.0 References

1. A. D. Compaan and R. G. Bohn, Annual Subcontract Report: High Efficiency Thin Film Cadmium Telluride Photovoltaic Cells, 20 Jan 1995--19 Jan. 1996. NREL/TP-451-21233. (Available from NTIS: publication DE96007892).

2. M. Shao, U. Jayamaha, E. Bykov, C.N. Tabory, and A.D. Compaan, "Performance vs. Microstructure in RF Sputtered CdS/CdTe Solar Cells," *Proc. 25th IEEE Photovoltaic Specialists Conference-1996*, (IEEE, Piscataway, N.J.) pp. 869-872.

3. M. Shao, A. Fischer, D. Grecu, U. Jayamaha, E. Bykov, G. Contreras-Puente, R.G. Bohn, and A.D. Compaan, Appl. Phys. Lett. **69**, 3045 (1996).

4. S.M Rossnagel, "Magnetron Plasma Deposition Processes," in *Handbook of Plasma Processing Technology*, edited by Rossnagel, Cuomo, and Westwood. (Noyes Publications, Park Ridge, N.J., 1990) pp. 160-182.

5. A.D. Compaan, R.G. Bohn, G. Contreras-Puente, C.N. Tabory, M. Shao, U. Jayamaha, A. Fischer, Z. Feng, C. Narayanswami, and D. Grecu, "High Efficiency Thin Film Cadmium Telluride Photovoltaic Cells," NREL Photovoltaic Program FY 1995 Annual Report.

6. Harris Semiconductor, 1700 Fostoria Road, Findlay, OH, 45840-6287.

7. Center for Surface Analysis of Materials, Case Western Reserve University, 10900 Euclid Ave., Clevelend, OH, 44106-7204.

8. Y.H. Kao, Dept. of Physics, State University of New York at Buffalo, Amherst, N.Y. 14260.

9. Dura Magnetics, 5500 Schulz Dr., Toledo, OH.

10. Chris Ferekides, Dept. of Electrical Engineering, Univ. of South Florida, 4202 E. Fowler Ave., Tampa, FL, 33620.

11. J.E. Granata, J.R. Sites, G. Contreras-Puente, & A.D. Compaan, "Effect of CdS Thickness on CdS/CdTe Quantum Efficiency," *Proc. 25th IEEE Photovoltaic Specialists Conference-1996*, (IEEE, Piscataway, N.J.) pp. 853-856.

12. D.G. Jensen, B.E. McCandless, and R.W. Birkmire, "Thin Film Cadmium Telluride-Cadmium Sulfide Alloys and Devices," *Proc. 25th IEEE Photovoltaic Specialists Conference-1996*, (IEEE, Piscataway, N.J.) pp. 773-776.

13. A. Aydinli, G. Contreras-Puente, A. Bhat, A. Compaan, and A. Chan, J. Vac. Sci. Technol. A, **9**, 3031 (1991).

14. A. Fischer, Z. Feng, E. Bykov, G. Contreras-Puente, A. Compaan, F.Castillo-Alvarado, J. Avendaño, and A. Mason, "Optical phonons in laser-deposited CdS_xTe_{1-x} films," Appl. Phys. Lett. (to be published June, 1997).

15. L. Genzel, T.P. Martin, and C.H. Perry, Phys. Stat. Sol. B, **62**, 83 (1974).

16. Yu.A. Mityagin, V.G. Plotnichenko, L.K. Vodop'yanov, and L.D. Budennaya, Sov. Phys. Solid. State., **19**, 1811 (1977).

17. A. Aydinli, A. Compaan, G. Contreras-Puente, and A. Mason, Sol. St. Commun. **80**, 465 (1991).

18. D.N. Talwar, Z.C. Feng, P. Becla, Phys. Rev. B, **48**, 17064 (1993).

19. R.G. Alonso, E.-K. Suh, A.K. Ramdas, N. Samarth, H. Luo, and J.K. Furdyna, Phys. Rev. B, **40**, 3720 (1989).

20. J. Avendaño-López, F.L. Castillo-Alvarado, A. Escamilla-Esquivel, G. Contreras-Puente, J. Ortiz-López, and O. Zelaya-Angel, Sol. St. Commun. **100**, 33 (1996).

21. A.D. Compaan, Z. Feng, G. Contreras-Puente, C. Narayanswami, and A. Fischer, Mat. Res. Soc. Symp. Proc. **426**, 367 (1996).

22. K. Ohata, J. Saraie, and T. Tanaka, Jpn. J. Appl. Phys. **12**1641 (1973).

23. P. Parayanthal and F.H. Pollak, Phys. Rev. Lett. **52**, 1822 (1984).

24. A. Fischer, C. Narayanswamy, D.S. Grecu, E. Bykov, S.A. Nance, U.N. Jayamaha, G. Contreras-Puente, A.D. Compaan, "Interdiffusion of CdS/CdTe in Laser Deposited and RF Sputtered Alloys, Bilayers, and Solar Cells," *Proc. 25th IEEE Photovoltaic Specialists Conference-1996*, (IEEE, Piscataway, N.J.) pp. 921-924.

25. Computer Graphic Service, Ltd., Ithaca, N.Y. 14850-8716.

26. A. D. Compaan and R. G. Bohn, "High Efficiency Thin Film Cadmium Telluride Photovoltaic Cells," Annual Subcontract Report, 20 Jan 1994--19 Jan. 1995 NREL/TP-451-8120. [Available NTIS: Order No. DE95009256].

28. Eugene Bykov, M.S. thesis, Univ. of Toledo, 1997 "Capacitance Measurements for Quantitative Analysis of Sputtered CdTe Solar Cells" (unpublished).

29. Meilun Shao, Ph.D. Thesis, Univ. of Toledo, 1995 "CdTe and CdS Thin Film Preparation Using RF Planar Magnetron Sputtering" (unpublished).

30. H.J. Queisser, Proc. of the Seventeenth International Conference on the Physics of Semiconductors, edited by D.J. Chadi (Springer-Verlag, NY, 1985)

31. J.W. Orton, B.J. Goldsmith, J.A. Chapman, and M.J. Powell, J. Applied Phys. 53, 1602 (1982)

12.0 Publications

Refereed papers published or in press (1/96-1/97):

1. M. Shao, A. Fischer, D. Grecu, U. Jayamaha, E. Bykov, G. Contreras-Puente, R.G. Bohn, and A.D. Compaan, Appl. Phys. Lett. **69**, 3045 (1996).

2. A. Compaan, M. Shao, A. Fischer, D. Grecu, U. Jayamaha, G. Contreras-Puente, & R.G. Bohn, Mat. Res. Soc. Symp. Proc. **426**, 391-396 (1996).

3. A.D. Compaan, Z. Feng, G. Contreras-Puente, C. Narayanswamy, & A. Fischer, "Properties of Pulsed Laser Deposited CdSxTel-x Films on Glass," Mat. Res. Soc. Symp. Proc. **426**, 367-371 (1996).

4. M. Shao, U. Jayamaha, E. Bykov, C.N. Tabory, and A.D. Compaan, "Performance vs. Microstructure in RF Sputtered CdS/CdTe Solar Cells," *Proc. 25th IEEE Photovoltaic Specialists Conference-1996*, (IEEE, Piscataway, N.J.) pp. 869-872.

5. A. Fischer, C. Narayanswamy, D.S. Grecu, E. Bykov, S.A. Nance, U.N. Jayamaha, G. Contreras-Puente, A.D. Compaan, "Interdiffusion of CdS/CdTe in Laser Deposited and RF Sputtered Alloys, Bilayers, and Solar Cells," *Proc. 25th IEEE Photovoltaic Specialists Conference-1996*, (IEEE, Piscataway, N.J.) pp. 921-924.

6. J.E. Granata, J.R. Sites, G. Contreras-Puente, & A.D. Compaan, "Effect of CdS Thickness on CdS/CdTe Quantum Efficiency," *Proc. 25th IEEE Photovoltaic Specialists Conference-1996*, (IEEE, Piscataway, N.J.) pp. 853-856.

7. D.H. Levi, B.D. Fluegel, R.K. Ahrenkiel, A.D. Compaan, & L.M. Woods,"Effect of CdS Thickness on CdS/CdTe Quantum Efficiency," *Proc. 25th IEEE Photovoltaic Specialists Conference-1996*, (IEEE, Piscataway, N.J.) pp. 913-916.

8. A. Fischer, U.N. Jayamaha, E. Bykov, D. Grecu, R.G. Bohn, & A.D. Compaan, *14th NREL/SNL PV Program Review* (AIP Conference Proceedings, to be published.)

Annual Subcontract Report:

1. A. D. Compaan and R. G. Bohn, Annual Subcontract Report: High Efficiency Thin Film Cadmium Telluride Photovoltaic Cells, 20 Jan 1995--19 Jan. 1996. NREL/TP-451-21233. (Available from NTIS: publication DE96007892).

Annual Reports published in NREL Annual Report, PV Subcontract Program:

1. A.D. Compaan, R.G. Bohn, G. Contreras-Puente, C.N. Tabory, M. Shao, U. Jayamaha, A. Fischer, Z. Feng, C. Narayanswami, and D. Grecu, "High Efficiency Thin Film Cadmium Telluride Photovoltaic Cells," NREL Photovoltaic Program FY 1995 Annual Report.

2. A.D. Compaan, R.G. Bohn, U. Jayamaha, A. Fischer, D. Grecu, E. Bykov, C. Narayanswamy, and D. Zuo, "High Efficiency Thin Film Cadmium Telluride Photovoltaic Cells," NREL Photovoltaic Program FY 1996 Annual Report (to be published).

13.0 Visiting Faculty, Students, and Research Assistants Participating in the Project

Visiting faculty member:

Gerardo Contreras-Puente has participated in this project with University of Toledo support until July 1996 while on sabbatical leave from the Polytechnic Institute in Mexico City.

Postdoctoral Associate: (-9/96)

Upali Jayamaha

Students:

Andreas Fischer
Ph.D. December 1996 "Photoluminescence and Raman Studies of CdTe, CdS_xTe_{1-x}, Alloys and CdS/CdTe Thin-Film Solar Cells"

Eugene Bykov
M.S. expected Mar. 1997 "Capacitance Measurements for Quantitative Analysis of Sputtered CdTe Solar Cells"

Dan Grecu
Ph.D. in progress

David Zuo
M.S. in progress

Chitra Narayanswamy
M.S. in progress

Technical Assistant: (1/95--8/95)

Robert Burmeister (4/96-) (25% time)

REPORT DOCUMENTATION PAGE

Form Approved
OMB NO. 0704-0188

1. AGENCY USE ONLY (Leave blank)	2. REPORT DATE	3. REPORT TYPE AND DATES COVERED
	August 1997	Annual Technical Progress Report, 20 January 1996 - 19 January 1997

4. TITLE AND SUBTITLE
High-Efficiency Thin-Film Cadmium Telluride Photovoltaic Cells, Annual Technical Report, 20 January 1996 - 19 January 1997

5. FUNDING NUMBERS
C: ZAX-4-14013-4
TA: PV704401

6. AUTHOR(S)
A.D. Compaan, R.G. Bohn, and G. Contreras-Puente

7. PERFORMING ORGANIZATION NAME(S) AND ADDRESS(ES)
Department of Physics and Astronomy
University of Toledo
Toledo, OH 43606

8. PERFORMING ORGANIZATION REPORT NUMBER

9. SPONSORING/MONITORING AGENCY NAME(S) AND ADDRESS(ES)
National Renewable Energy Laboratory
1617 Cole Blvd.
Golden, CO 80401-3393

10. SPONSORING/MONITORING AGENCY REPORT NUMBER
SR-520-23404

11. SUPPLEMENTARY NOTES
NREL Technical Monitor: B. von Roedern

12a. DISTRIBUTION/AVAILABILITY STATEMENT

12b. DISTRIBUTION CODE
UC-1263

13. ABSTRACT *(Maximum 200 words)*

The University of Toledo (UT) photovoltaics group was instrumental in developing radio-frequency (rf) sputtering for CdS/CdTe thin-film solar cells. During the third phase of the present contract, the work focused on efforts to determine factors that limit the efficiency in "all-sputtered" thin-film CdTe solar cells on soda-lime glass. Researchers found that all-sputtered cells, which are deposited at substantially lower temperature than those by sublimation or vapor deposition, require less aggressive $CdCl_2$ treatments than do other deposition techniques and this is presumably related to CdS/CdTe interdiffusion. The CdS/CdTe interdiffusion has been studied by several methods, including photoluminescence and capacitance-voltage measurements. Researchers also deposited special thin bilayer films on quartz and borosilicate glass. Also, to better understand the properties of the ternary alloy material, they used laser physical vapor deposition to prepare a series of CdS_xTe_{1-x} films on borosilicate glass. In addition to efforts focused on factors that may be unique to rf-sputtered cells, researchers participated in activities emphasizing common issues in CdTe thin-film solar cells. Researchers prepared cells on both 7059 borosilicate glass with conducting tin oxide layers deposited at the University of South Florida (USF) and on soda-lime glass with textured SnO_2 from LOF. Including the work from the previous phase, researchers have now fabricated seven types of cells with CdS thicknesses of 300, 200, 100, 80, 60, 20, and 0 nm. For each CdS thickness, cells on the 7059 and soda-lime superstrates were prepared side-by-side through all steps in the preparation to facilitate direct comparisons. The 7059/USF SnO_2 superstrates had much better performance for CdS thicknesses of 100 nm and below, with the major differences occurring in the open-circuit voltage. One set of cells prepared without CdS by sputtering CdTe directly on the 7059 USF SnO_2 superstrates showed an initial V_{oc} of 760 mV and initial efficiency of 8.7%. Other characterization measurements in use at UT include temperature-dependent Hall effect and electrical conductivity, current-voltage (I-V), spectral quantum efficiency (SQE), and frequency-dependent capacitance-voltage (C-V) measurements.

14. SUBJECT TERMS
photovoltaics ; high-efficiency thin films ; cadmium telluride ; photovoltaic cells ; borosilicate glass

15. NUMBER OF PAGES
4 43

16. PRICE CODE

17. SECURITY CLASSIFICATION OF REPORT	18. SECURITY CLASSIFICATION OF THIS PAGE	19. SECURITY CLASSIFICATION OF ABSTRACT	20. LIMITATION OF ABSTRACT
Unclassified	Unclassified	Unclassified	UL